



1 Moss kill-dates and modeled summer temperature track episodic snowline
2 lowering and ice-cap expansion in Arctic Canada through the Common Era

3
4 ^{1,2}Gifford H. Miller, ³Simon L. Pendleton, ^{1,4}Alexandra Jahn, ⁵Yafang Zhong, ¹John T. Andrews,
5 ¹Scott J. Lehman, ⁶Jason P. Briner, ^{1,2}Jonathan H. Raberg, ⁷Helga Bueltmann, ⁸Martha
6 Reynolds, ⁹Áslaug Geirsdóttir, and ¹⁰John R. Southon

7
8 ¹Institute of Arctic and Alpine Research University of Colorado Boulder, Boulder, CO 80303, USA

9 ²Department of Geological Sciences, University of Colorado Boulder, Boulder, CO 80303, USA

10 ³Environmental Science and Policy Program, Plymouth State University, Plymouth, NH 03264, USA

11 ⁴Department of Atmospheric and Oceanic Sciences, University of Colorado Boulder, Boulder, CO 80303, USA

12 ⁵Space Science & Engineering Center, University of Wisconsin-Madison, Madison, WI 53706, USA.

13 ⁶Department of Geology, University at Buffalo, Buffalo, NY, USA

14 ⁷Institute of Biology and Biotechnology of Plants, University of Münster, Münster, Germany

15 ⁸Institute of Arctic Biology, University of Alaska Fairbanks, Fairbanks, AK, USA

16 ⁹Institute of Earth Sciences and Department of Earth Sciences, University of Iceland, Reykjavik 101, Iceland

17 ¹⁰W.M. Keck Carbon Cycle AMS Laboratory, University of California at Irvine, Irvine, CA, USA

18
19 **Correspondence to:** Gifford H. Miller (gmiller@colorado.edu)

20
21
22 **ABSTRACT**

23
24 Most extant ice caps mantling low-relief Arctic Canada landscapes remained cold-based
25 throughout the late Holocene, preserving *in situ* bryophytes killed as ice expanded across
26 vegetated landscapes. As Arctic summers warmed after 1900 CE, ice caps receded, exposing
27 entombed vegetation. The calibrated radiocarbon ages of dead moss collected near ice-cap
28 margins (kill-dates) define when ice advanced across the site, killing the moss, and remained
29 over the site until the year of their collection. In an earlier study we reported 94 Last
30 Millennium radiocarbon dates on *in situ* dead moss collected at ice-cap margins across Baffin
31 Island, Arctic Canada. Tight clustering of those ages indicated an abrupt onset of the Little Ice
32 Age ~1240 CE, and further expansion ~1480 CE, coincident with episodes of major explosive
33 volcanism. Here we test the confidence in kill dates as reliable predictors of expanding ice
34 caps by re-sampling two previously densely-sampled ice complexes 14 years later, after ~250
35 m of ice recession. The probability density functions (PDF) of the more recent series of ages
36 matches PDFs of the earlier series, but with a larger fraction of early CE ages. Post 2005 CE
37 ice recession has exposed relict ice caps that grew during earlier Common Era advances, and
38 were preserved beneath later ice-cap growth. We compare 107 kill dates from the two ice
39 complexes with 79 kill dates from 62 other ice caps within 250 km of the two densely sampled
40 ice complexes. The PDF of kill dates from the 62 other ice caps cluster in the same time
41 windows as those from the two ice complexes alone, with the PDF of all 186 kill dates
42 documenting episodes of widespread ice expansion restricted almost exclusively to 250-450
43 CE, 850-1000 CE and a dense early Little Ice Age cluster with peaks at ~1240 and ~1480 CE.



44 Ice continued to expand after 1480 CE, reaching maximum dimensions ~1880 CE, still visible
45 as zones of sparse vegetation cover in remotely sensed imagery. Intervals of widespread ice-
46 cap expansion coincide with persistent decreases in mean summer surface air temperature
47 for the region in a Community Earth System Modeling (CESM) fully coupled Common Era
48 simulation, suggesting primary forcing of the observed snowline lowerings were both modest
49 declines in summer insolation, and cooling resulting from explosive volcanism, most likely
50 intensified by positive feedbacks from sea-ice expansion and reduced northward heat
51 transport by the oceans. The clusters of ice-cap expansion defined by moss kill-dates are
52 mirrored in an annually resolved Common Era record of ice-cap dimensions in Iceland,
53 suggesting this is a circum-North-Atlantic-Arctic climate signal for the Common Era. During
54 the coldest century of the Common Era, 1780-1880 CE, ice caps mantled >11,000 km² of
55 north-central Baffin Island, whereas <100 km² is glaciated at present. The peak Little Ice Age
56 state approached conditions expected during the inception phase of an ice age, and was only
57 reversed after 1880 CE by anthropogenic alterations of the planetary energy balance.

58

59 1. INTRODUCTION

60

61 The Canadian Arctic Archipelago (CAA) supports nearly 150,000 km² of glaciers and
62 independent ice caps, the greatest concentration of land ice outside Greenland and
63 Antarctica (Medrzycka et al., 2022). As Earth warms, regardless of forcing mechanism, strong
64 positive feedbacks in the Arctic result in greater temperature increases there relative to the
65 planetary average on all timescales (Miller et al., 2010). Consistent with that, the rate of
66 contemporary warming for the Arctic is greater than for most other geographic regions
67 (Rantanen et al., 2022), particularly across the North Atlantic sector (Zhong et al., 2018). All
68 CAA glaciers are now losing mass as summers continue to warm (Gardner et al., 2012;
69 Lenaerts et al, 2013; Noël et al., 2018). In a review of controls on glacier mass balance in the
70 CAA, Koerner (2005) demonstrated that summer temperature explains ~95% of annual mass
71 balance variations over the previous 40 years of record, with the winter mass balance having
72 negligible explanatory power. Consequently, changes in glacier dimensions dominantly
73 reflect changes in summer temperature, and changes in glacier dimensions over time provide
74 one of the most reliable records for the evolution of past summer temperatures. Unlike
75 biological proxies that require evaluating an organism's adaptations to mitigate climate
76 stressors, glaciers have no strategy for survival. If it snows more in winter than melts in
77 summer, non-calving glaciers expand; conversely if more mass is lost by summer melt than is
78 gained through winter snowfall, they recede.

79 Baffin Island, the largest island in the Canadian Arctic, is an elongate tilted
80 Precambrian block, stretching ~1600 km paralleling the west coast of Greenland. The island
81 was inundated by the Laurentide Ice Sheet (LIS) at the last glacial maximum. Although
82 deglaciation proceeded rapidly under high summer insolation in the early Holocene, our field
83 area (Fig. 1), remained beneath the residual ice sheet 7000 years ago, and probably was not
84 free of Laurentide ice until after 5 ka (Dyke, 2004). The Barnes Ice Cap, at the southern edge



85 of our field area, is a remnant of the LIS, and the coastal highlands east of our field area never
86 fully deglaciated in the Holocene (Pendleton et al., 2019a).

87 Our primary focus is the 30,000 km² north-central uplands inscribed in Fig. 1, which
88 rise gradually from sea level at the west coast to ~900 m asl inland, after which they rise
89 rapidly to the high-elevation, deeply dissected fiord country along the east coast, where the
90 interfluves are mantled by large ice caps and cirque glaciers. In contrast, isolated small, thin
91 ice caps currently cover ~100 km² of the highest summits across the low-relief uplands.
92 Vegetation is sparse, dominated by lichens and bryophytes, with less common vascular
93 plants. The only woody plants are prostrate species of willow (*Salix*). Our sampled ice caps
94 (Fig. 1) occur across a larger region of about 55,000 km².

95

96 2. NEOGLACIATION

97

98 Although deglaciation of the Laurentide Ice Sheet from Baffin Island continued through most
99 of the Holocene, the orbitally driven decline of Northern Hemisphere summer insolation after
100 ~11 ka resulted in a lowering of snowline and high-elevation ice-cap expansion as early as 9
101 ka (Lecavalier et al., 2017; Pendleton et al., 2017). Local ice cap and cirque glaciers were
102 advancing by 5 ka (Moore et al., 2001), considered the onset of Neoglaciation, with ice
103 expansion widespread by ~3 ka (Miller, 1973). In response to the continuing decline in
104 Northern Hemisphere summer insolation, Baffin Island ice caps reached their maximum
105 dimensions during the Little Ice Age (1240-1900 CE), the coldest centuries of the Holocene
106 (Miller et al., 2012). Initial dating of Neoglacial ice margins was by lichenometry (Miller, 1973;
107 Locke and Locke, 1977; Davis, 1985) and subsequently based on cosmogenic isotopes in
108 moraine boulders (Anderson, et al., 2008; Briner et al., 2009; Crump et al., 2017). Continuous
109 records of Neoglacial activity on Baffin Island are derived from lake sediment cores (Moore
110 et al., 2001; Miller et al., 2005; Briner et al., 2006; Briner et al., 2016), all confirming maximum
111 ice dimensions during the Little Ice Age. Ives (1957; 1962) was the first to recognize that
112 spectral differences in aerial imagery of northern Baffin Island uplands indicated that sparsely
113 vegetated regions reflected a Little Ice Age (LIA) lowering of snowline that killed all vegetation
114 across, and that early 20th Century warming had reduced an extensive LIA ice complex to a
115 few small remaining ice caps that mantle the highest summits (Williams, 1978). Wolken et al.
116 (2005) evaluated the evidence for and against permanent ice cover explaining the sparsely
117 vegetated zones, concluding that permanent ice cover was indeed the most likely cause.
118 Although re-vegetation is rapidly occurring, the spectral signal remains preserved in recent
119 satellite imagery (Fig. 2), although less distinct than in imagery from the 1950s. Andrews et
120 al. (1975; 1976) used the light-toned areas on air photos and satellite imagery to produce the
121 first map of perennial ice-cover over north-central Baffin Island at the peak of the Little Ice
122 Age. However, the dating of the LIA snowline minimum remains uncertain.

123 Falconer (1966) was the first to recognize that the receding upland ice caps were
124 frozen to their beds. Rather than active erosive agents, they are exceptional preservation
125 agents. Bedrock striae appearing as contemporary ice recedes, show ice flow to the NE



126 around all margins of current ice caps, reflecting only regional Laurentide Ice Sheet flow at
127 the last glacial maximum (Dyke, 2004). Striae, relict patterned ground (Falconer, 1966),
128 delicately perched erratic boulders appearing as contemporary ice surfaces lower (Fig. 3), and
129 the lack of englacial debris confirm cold-based ice. As ice caps recede, they also reveal
130 entombed vegetation in position of growth. The radiocarbon ages of dead moss are “kill
131 dates”, that define when ice expanded across the site, killing vegetation, and then remained
132 over the site, preserving the dead plants until ice recession. Once exposed, dead vegetation
133 is efficiently removed by meltwater or wind-blown snow within a few years, although in rare
134 settings devoid of meltwater, they are known to persist for several decades (e.g., Miller et al.,
135 2017; Pendleton et al., 2017). Falconer (1966) reported the first radiocarbon date on *in situ*
136 dead moss collected at the margin of Tiger Ice Cap (Fig. 2), 330 ± 75 yr BP (I-1204), confirming
137 ice expansion occurred during the Little Ice Age, but the precision is too low to include here.
138 Miller visited the same ice cap in 1981, collecting moss at the ice edge that returned a ^{14}C age
139 of 460 ± 25 (GSC-5025), early in the Little Ice Age.

140 Here we report 186 calibrated radiocarbon dates on dead moss collected at the
141 margins of receding ice caps that mantle summits across the uplands of northern Baffin
142 Island, including all 107 ice-marginal dates within the area inscribed in Fig. 1, and an
143 additional 79 CE dates from 62 other local glaciers and ice caps in the adjacent high-elevation
144 mountainous regions (Fig. 1). Moss “kill-dates” define when an adjacent ice cap advanced
145 across the site during an episode of cooler summers, and remained over the site for decades,
146 killing the moss. We report kill-dates from two densely sampled ice-cap complexes, each
147 sampled ~ 15 years apart, and compare those ages with Common Era dates from 62 other ice
148 caps within 250 km of the densely sampled ice complexes. Three age clusters defined by the
149 probability density functions (PDF) of the composited 186 kill-dates are compared with mean
150 summer temperatures simulated in a fully coupled climate model for the Common Era (CESM
151 past2k; Zhong et al., 2018). The kill-date clusters correspond to century-scale anomalously
152 cold summers in the model, whereas gaps between kill-date clusters are relatively warm
153 summers in the model. The close correspondence between modeled summer temperatures
154 and changes in ice-cap dimensions, allows us to constrain the age of previously undated, low-
155 elevation, sparsely vegetated zones that define an interval of extensive ice-cap cover at
156 elevations up to 400 m below extant ice caps.

157 We conclude that ice caps throughout the field area expanded to increasingly lower
158 elevations between 250 and 450 CE, 850 and 1000 CE, and 1240 to 1480 CE, eventually
159 reaching maximum coverage at lowest elevations between 1780 and 1880 CE, effectively
160 resulting in “instantaneous glacierization”, a condition predicted to be the prelude to an ice-
161 age cycle. Anthropogenic influences on the planetary energy balance after 1850 CE likely
162 thwarted any possibility of a new ice age, despite optimal orbital configuration for glacial
163 inception.

164

165 3. METHODS

166



167 We built on the pioneering work of Ives, Andrews, and Falconer beginning in 2005, collecting
168 *in situ* dead moss, usually within a meter of the ice margin at the time of collection. We
169 concentrated our field studies on the low-relief upland of north-central Baffin Island between
170 the Barnes Ice Cap and Lancaster Sound (Fig. 1), with permission from the Qikiqtani Inuit
171 licensed through the Nunavut Research Institute. We densely sampled two ice complexes
172 mantling the highest uplands: the Serpens Ice Complex (SRP) consisting of three primary ice
173 caps, and the Orion Ice Complex (ORN; both unofficial names), consisting of six ice caps in
174 2005 (Fig. 2). Additional collections were made in 2009, 2010, 2018, and 2019.

175

176 3.1 Radiocarbon dated moss.

177 Our primary data set is the radiocarbon ages of *in situ* ice-edge dead moss. Ice-margin retreat
178 rates were measured at $\sim 10 \text{ m a}^{-1}$, and $\geq 1 \text{ m a}^{-1}$ vertical lowering (2006-2008 CE), confirming
179 vegetation collected a few meters from the ice margin was exposed during the year of
180 collection. Regions where similar studies use moss kill dates to reconstruct the timing of
181 Neoglacial ice cap expansion include Franz Josef Land (Lubinski et al., 1999), Svalbard (Miller
182 et al. 2017), Greenland (Lowell et al., 2013; Medford et al., 2021; Schweinsberg et al., 2017;
183 2018; Søndergaard et al., 2019), Baffin Island (Falconer, 1966; Anderson et al., 2008; Miller
184 et al., 2013; Margreth et al., 2014; Pendleton, 2019a&b), Alaska (Calkin and Ellis, 1981),
185 Iceland (Harning et al., 2016), and Antarctica (Yu et al., 2016; Groff et al., 2023).

186 We target members of the widespread moss family Polytrichaceae, primarily the
187 genus *Polytrichum*, which has a thickened central stem of sufficient mass that a single stem
188 is adequate for a precise AMS ^{14}C date. We previously showed that the ^{14}C concentration in
189 living *Polytrichum* is in equilibrium with that of the contemporary atmosphere, that ^{14}C dates
190 on different *Polytrichum* stems in a single clump are statistically indistinguishable, confirming
191 that they grow relatively quickly, and that ^{14}C dates on *Polytrichum* collected at four sites
192 along 200 m of a modern ice cap margin are statistically indistinguishable (Supplemental Fig.
193 1). These datasets support the interpretation that the timing of ice-cap expansion can be
194 reliably reconstructed from the ^{14}C kill dates on *in situ* dead *Polytrichum* and other mosses
195 revealed as ice caps recede under contemporary warming. We note, however, that very
196 different kill dates can occur over ice-margin distances of a few tens of meters, when the
197 receding ice margin intercepts a buried, older ice cap, preserved beneath a more recent ice
198 expansion.

199 Although *Polytrichum* is the most common moss appearing as ice margins recede, if
200 *Polytrichum* is not present, we rely on *Andreaea*, a genus of small rock mosses that commonly
201 grow on siliceous rocks; they represent 9% of the dated samples. Because they are small,
202 multiple strands are required for dating. Another 30% of the dated samples were collected
203 before we gave taxonomic names to moss collections; they are almost all likely to be
204 Polytrichaceae. Radiocarbon dates on co-located lichens are always older and are not
205 included here. In the lab, plant samples are sonicated in de-ionized water, then freeze-dried.
206 From the freeze-dried samples sufficient material ($\sim 2 \text{ mg}$) was separated and submitted for
207 dating. Combustion and graphitization of cleaned CO_2 is accomplished in INSTAAR's



208 Laboratory for AMS Radiocarbon Preparation and Research (NSRL) and measured at the W.
209 M. Keck Carbon Cycle Accelerator Mass Spectrometry Laboratory at the University of
210 California, Irvine; a few samples were measured at the National Ocean Sciences Accelerator
211 Mass Spectrometry at Woods Hole Oceanographic Institution. Radiocarbon dates were
212 calibrated using OxCal 4.2.4 and IntCal20 (Bronk Ramsey, 2009; Reimer et al., 2020) and
213 expressed in years CE. Some of our dates were reported previously using IntCal13, resulting
214 in small changes in the calibrated age distributions in this paper. The OxCal program reports
215 the probability as a percentage for each year provided by the calibration process. For
216 collections of interest, we sum the yearly probabilities, then normalize and plot as a
217 probability density function (PDF). Samples from multiple years and from different regions
218 can be aggregated and effectively compared this way. A complete tabulation of sample
219 details and calibrated ages for all 186 samples used in this report is available at the NSF Arctic
220 Data Center (<https://arcticdata.io>).

221

222 3.2 Climate Modeling

223 We make use of the CESM1-CAM5 (Hurrell et al., 2013) “past2k” transient climate simulation
224 of the Common Era (1-2005 CE) (Zhong et al., 2018 GRL). This simulation has 2° resolution in
225 the atmosphere and land and ~1° resolution in the ocean and sea ice, the same configuration
226 as used for the CESM Last Millennium Ensemble (LME; Otto-Bliesner et al., 2016). We extract
227 the simulated summer (JJA) 2-m air temperature averaged over North Atlantic Arctic land
228 areas (>60°N and between 90°W and 30°E) through the Common Era (1-2005 CE).

229 The past2k forcing data (Fig. 4) were mostly from the Paleoclimate Model
230 Intercomparison Phase 4 project (PMIP4; Jungclaus et al., 2017) for the Coupled Model
231 Intercomparison Project Phase 6. They include changes in solar irradiance and insolation,
232 volcanic aerosols (Toohey et al., 2016), and greenhouse gas levels (MacFarling et al., 2006).
233 The land-cover forcing for the past2k simulation from 850 CE to 2005 CE is taken from the
234 LME, which implements changes in grassland and cropland as compiled by PMIP3. The land
235 cover forcing from 1 to 849 CE is a superposition of HYDE3.1 cropland changes (Goldewijk et
236 al., 2011) onto the land cover forcing from the LME for 850 CE (see Zhong et al., 2018 for full
237 details).

238 For us to assess the importance of anthropogenic activities in terminating the Little
239 Ice Age, we also use existing CESM1-CAM5 simulations at ~1° resolution in all model
240 components for 1850-2005. Specifically, we make use of the simulated summer temperatures
241 from four simulations with all forcings (Hurrell et al. 2013), the standard “Historical” forcing
242 used for the CESM1 CMIP5 simulations. In addition, we also use the summer temperatures
243 from three simulations with only “Natural” forcings. The “Natural” forcing experiment is
244 forced only by solar variability and volcanic aerosol emissions, following the CMIP5 protocol
245 (Taylor et al., 2012), and is part of a published dataset of single forcing experiments with the
246 CESM1-CAM for 1850-2005 that were previously used in other studies (Meehl et al., 2020;
247 Taylor et al., 2012; Xu et al. 2022). By using all available ensemble members from these two



248 experiments, we can assess the impact of the anthropogenic forcing beyond the influence of
249 internal variability.

250

251 **4. RESULTS**

252

253 4.1 Repeat sampling around the ORN and SRP ice complexes

254 In 2005 we collected dead moss around the margins of the Orion (ORN: 18 dated samples)
255 and Serpens (SRP: 22 dated samples, 4 collected in 2009) ice complexes (Fig. 2). The
256 composite PDF of both datasets showed clusters of similar kill dates (Miller et al., 2012). To
257 test whether those clusters were artifacts of the state of the ice caps during the year of
258 collection, we re-sampled ORN in 2018, and SRP in 2019, after ~250 m of ice recession at
259 both, and with a greater sampling density.

260

261 4.1.1 Orion Ice Complex (Fig. 2) The 2005 moss kill-dates (Fig. 5A) cluster between
262 850 and 1000 CE and 1240 to 1480 CE, with a scattering of dates between the two clusters.
263 The PDF of 33 kill dates collected in 2018 (Fig. 5B) is broadly similar, with dominant clusters
264 between 850 and 1000 CE, and between 1240 and 1500 CE, but also an older cluster between
265 250 and 450 CE. In the 2005-2018 composite PDF (Fig. 5C) the older cluster reflects moss
266 killed during an early First Millennium expansion of ORN, that likely melted partially after 450
267 CE, but never completely disappeared. The residual early First Millennium ice cap was
268 subsumed by a late First Millennium expansion beginning ca. 850 CE, and preserved beneath
269 younger ice, only to re-emerge and re-start recession under contemporary warming,
270 exposing plants killed during the early First Millennium ice expansion. A primary conclusion
271 from these data is that summer temperatures over the past century are warmer, on average,
272 than any century since 450 CE. The 2018 glacier where ice-marginal moss produced early First
273 Millennium ages has surface characteristics visible in high-resolution imagery captured for us
274 by Digital Globe that differ in character from the glacier surface farther along the ice margin
275 in either direction where the moss kill dates are much younger, supporting our interpretation
276 that in 2018 a remnant early first millennium ice cap that never melted completely was
277 emerging from beneath a younger ice cap that grew when snowline subsequently fell across
278 the region. The near identical alignment of the two younger 2018 clusters with those from
279 2005 confirms the utility of moss kill dates as reliable ages of Common Era ice-cap expansion,
280 regardless of collection date.

281

282 4.1.2 Serpens Ice Complex The PDFs of the 2005/2009 (22 dates) and 2019 (34 dates)
283 collections from SRP (Fig. 6 A&B) produce clusters in nearly identical time intervals, and that
284 match clusters in the ORN composite PDF (Fig. 5C): 250 to 450 CE, 850 to 1000 CE and 1240
285 to 1480 CE.

286

287 4.1.3 The SRP+ORN PDF (Fig. 4-3) The PDFs for all dates from SRP (Fig. 7A) and from
288 ORN (Fig. 7B) are combined as the SRP+ORN composite (Fig. 7C), consisting of 107 calibrated



289 ¹⁴C dates. That PDF produces three well-defined clusters, reflecting an early first millennium
290 expansion between 250 and 450 CE found in 5 samples from SRP and 3 from ORN. There is
291 virtually no evidence of ice expansion between 450 and 850 CE, after which both ice
292 complexes show expanding margins from 850 to 1000 CE (11 from ORN and 12 from SRP).
293 ORN yielded 6 samples scattered between 1050 and 1160 CE, but with no central tendency,
294 whereas SRP has none. However, both SRP and ORN have large numbers of dates beginning
295 ~1240 CE and ~780 CE is related to calibration. Radiocarbon ages between 1080 and 1180 yr
296 BP have continuing until ~1480 CE (25 from ORN and 37 from SRP), indicating ice margins
297 expanded throughout that interval.

298 In both SRP and ORN composite PDFs (Fig. 7) a sharply defined peak centered on ~780
299 CE is related to calibration. Radiocarbon ages between 1080 and 1180 yr BP have median
300 calibrated ages between 850 and 960 CE, but they all also have a small (<~5%) probability of
301 an age clustered tightly around 780 CE. Because 21% of the radiocarbon ages the 109
302 radiocarbon dates from the two complexes are between 1080 and 1180 yr BP, their
303 calibration creates a low probability but strongly expressed peak clustered tightly around 780
304 CE. Because of the low probability that this is the actual calibrated age, and lacking other
305 samples in the same time range, we consider it highly unlikely that 780 CE is an interval of
306 expanding ice caps.

307 We test the potential for variations in atmospheric ¹⁴CO₂ concentrations to have
308 influenced the structure of the SRP+ORN PDF by creating 160 random radiocarbon ages
309 between 1 and 1500 CE with similar uncertainties (±25 years) as our moss dates. That
310 calibrated PDF is compared with the SRP+ORN composite PDF in Fig. 8. There are clear natural
311 biases in the random series, with artificial peaks centered on 660 and 1020 CE, time periods
312 where there is no power in the SRP+ORN PDF, but also peaks at about 1280 and 1480 CE,
313 which likely contribute to the height of those peaks in the SRP+ORN PDF, but do not alter the
314 conclusion that widespread ice-cap expansion occurred between 1240 and 1480 CE.

315

316 4.1.4 Testing the SRP+ORN Composite (Fig. 9) The combined SRP+ORN PDF defines
317 sustained Common Era ice-cap expansion limited to three primary intervals: 250 to 450 CE,
318 850 to 1000 CE and after 1240 CE. The SRP Complex consists of 3 independent ice caps,
319 whereas ORN consisted of 6 independent ice caps sampled in 2005, of which portions of only
320 3 remain. To test whether the densely sampled ice complexes reflect regional snowline
321 lowering across northern Baffin Island we collected 79 additional dead moss from the margins
322 of 62 other ice caps. Those additional ice caps include other small ice caps situated on low
323 relief landscapes similar to ORN and SRP, but also include low-relief summits within much
324 larger ice complexes where ice-expansion is primarily by vertical thickening rather than ice
325 flow. None of the samples are from outlet glaciers; all are within 250 km of SRP and ORN. We
326 avoid cirque glaciers because response times to snowline lowering are more complex than
327 for small upland ice caps or the vertical thickening of large ice caps, both of which change in
328 direct response to summer temperature and are largely unrelated to ice flow.



329 The resultant PDF of those 79 calibrated ages is compared with the PDF of the 107
330 dates from SRP+ORN in Fig. 9. The isolated ice cap dates (Fig. 9B) cluster primarily in the same
331 three groupings apparent in the SRP+ORN PDF (Fig. 9A), although the early first millennium
332 250-450 CE cluster is more strongly represented, and the onset extends to near the start of
333 the First Millennium. The three samples that contribute to that tail are from elevations above
334 900 m asl, higher than ORN and SRP, suggesting that summer cooling began earlier than
335 recorded by SRP+ORN, and that snowline did not drop below their elevations until after 250
336 CE, or that subsequent summer warmth fully melted all pre-CE advances. The 850-1000 CE
337 cluster is apparent in both data sets, and with similar overall structure, suggesting regional
338 climate forcing. Both data sets lack significant ice expansion between 1000 and 1240 CE, and
339 both exhibit evidence of widespread expansion beginning abruptly ~1240 CE and continuing
340 to ~1480 CE, with at least some of the spikiness of the PDF likely an artifact of the variations
341 in ¹⁴C concentration of atmospheric CO₂ across that time range (Fig. 8).

342 The large cluster of kill-dates 1240-1480 CE suggest snowline declined throughout
343 that interval. However, at multiple sites moss collected in 2005 have kill-dates ~1250 CE,
344 whereas in 2019, after ~200 m of ice recession, ice-margin moss have younger kill dates
345 (~1450 CE), requiring an interval of modest ice recession before a readvance late in that time
346 interval, with preservation of the older moss beyond the receded ice margin. These results
347 suggest this 240-year interval was not characterized by monotonic summer cooling; rather
348 summer cooling was interrupted by at least one episode of warm summers leading to ice
349 recession, without all moss killed by the initial advance eroded from the landscape. Because
350 dead moss are relatively easily eroded, the duration of ice-recession interval must have been
351 brief, no more than a few decades, and followed by rapid re-expansion of the ice cap(s).

352 The composite record consisting of 186 calibrated radiocarbon dates from 70 different
353 ice caps (Fig. 9C) constrains ice-cap expansion during the Common Era across northern Baffin
354 Island. The well-defined clusters suggest snowline began to decline early in the First
355 Millennium CE, resulting in widespread ice-cap expansion between 250 and 450 CE (21 dates).
356 There is no evidence from kill-dates for additional ice-cap growth until after 800 CE, with
357 widespread ice-cap expansion between 850 and 1000 CE (43 dates). There is little evidence
358 for snowline lowering during Medieval times, between 1000 and 1240 CE, but summer
359 temperatures were also not high enough then to raise the snowline above all ice caps that
360 formed earlier in the first millennium, or long enough, to cause those First Millennium ice
361 caps to disappear. This suggests that Medieval times were certainly not as warm, on average,
362 as the earliest centuries of the Common Era, but also that Medieval times experienced no
363 sustained decades of significant summer cold. 1240 CE marks the start of the Little Ice Age,
364 with clear evidence of intermittent ice-cap expansion in all datasets, continuing for the next
365 240 years (97 dates).

366 None of the kill-dates from plateau ice caps pre-date the Common Era. Consequently,
367 if earlier late Holocene episodes of summer cold resulted in long-lived ice caps across Baffin
368 Island uplands, subsequent summers were warm enough and/or long enough to completely
369 melt those ice caps before 1 CE. Our moss dates are relatively silent about the state of the ice



370 caps after ~1500 CE. We turn to climate models to derive information on ice cap dimensions
371 after ~1500 CE

372

373 4.2 Modeling the evolution of Common Era summer temperature

374 From the past2k model output we extract the evolution of summer (JJA) temperatures over
375 land areas north of 60°N that lie between 30°W and 90°E, capturing a broad representation
376 of North Atlantic Arctic lands, and including the climate impacts from sea-ice feedbacks.
377 Although climate is often approximated using a 30-year average, cold-based ice caps mantling
378 low-relief landscapes on Baffin Island have a longer, multi-decadal response time, so we use
379 a 50-year running mean for our data-model comparison. The 50-year running mean of
380 summer temperature through the Common Era exhibits a declining first-order trend up to
381 1890 CE (Fig. 10), consistent with the strong influence from declining NH summer insolation
382 from orbital terms. Because Baffin Island is only a portion of the land included in our
383 extraction of mean JJA summer temperatures (Fig. 10 Inset), the absolute values of modeled
384 temperatures are unlikely to match those of our field area, and we evaluate the relative
385 changes in summer temperature without regard to absolute values.

386 To assess how well the past2k summer temperatures represent the summer
387 temperature evolution in the study region, we compare the past2k summer temperatures
388 with a 50-year record of summer temperature from the only Baffin Island interior weather
389 station, Dewar Lakes, ~350 km SE of our field area, at 500 m asl. The mean summer (JJA)
390 temperature at Dewar Lakes from 1958-2022 exhibits high inter-annual variability (up to 5°C,
391 and a range of almost 9°C) but the 10-year running mean (Fig. 11) shows that relatively warm
392 summers in the 1950s were followed by colder summers in the 1960s and early 1970s, after
393 which variably warming summers dominate the record. The 5-year running mean summer
394 temperature record in our CESM past2k simulation for the period of overlap (1958-2005; Fig.
395 11) reasonably mimics the Dewar Lakes record, when accounting for the expected much
396 lower variability in the model results due to the averaging over a much larger area.

397 Both the Dewar Lakes recorded summer temperatures and CESM simulated summer
398 temperatures indicate cold summers in the 1960s and early 1970s. We compare those
399 records with ice-cap retreat rates for three ice caps (WT, SRP, ORN, Fig. 2) from remote
400 images spanning 1957-2020 CE. All three ice caps show reduced rate of aerial decrease
401 between 1960 and the early 1970s (Fig. 12), lending additional confidence to the simulated
402 summer temperatures in the past2k results. Summer warming in both Dewar Lakes and
403 past2k records since 1980 is matched by increased ice-cap recession rates. The close
404 correspondence between past2k modeled summer temperatures and the Dewar Lakes
405 recorded temperatures, and rates of ice-cap recession for WT, SRP, and ORN, provide a
406 measure of confidence in the CESM modeled summer temperatures through the Common
407 Era.

408

409 4.3 Comparing modeled summer temperatures with ice-cap kill dates.



410 Because summer temperature is the dominant control on Baffin Island glacier mass balance
411 (Koerner, 2005) we expect below average modeled summer temperatures to correspond
412 with episodes of ice cap expansion. The modeled 50-year mean summer temperatures (Fig.
413 10) contains significant centennial-scale structure. Primary forcings leading to the
414 temperature decline in the model (Fig. 4) include a reduction in Northern Hemisphere
415 summer insolation through the Common Era, small reductions in TSI between 1300 and 1700
416 CE, and episodes of sulfur-rich explosive volcanism with the associated positive feedbacks
417 from expanded sea ice, additional snow cover over land, and changes in ocean circulation.
418 Anthropogenic impacts become important after ~1850 CE.

419 A piecewise regression of JJA temperatures (1-1900 CE; Supplemental Figure 2)
420 suggests an initial steep decline from 1 to 900 CE, warming from 900 to 1050 CE, followed by
421 a slower decline between 1050 and 1900 CE. While the piecewise regression captures some
422 of the Common Era structure, it lacks the detail necessary to compare with the kill-date
423 composite PDF (Fig. 9C).

424 To more directly compare past2k 50-year mean summer temperatures with the
425 information provided by our moss kill dates, we instead calculate multi-century linear
426 regressions of modeled summer temperature across time periods of ice-cap and across
427 intervals lacking evidence of expanding ice caps expansion based on the kill dates (Fig. 10), to
428 better evaluate whether the climatic implications of kill-dates align with modeled summer
429 temperatures. This relaxes the constraints for piecewise regressions that requires individual
430 regressions be continuous. The linear regression through mean summer temperatures
431 between 250 and 450 CE defines a steady decline in summer temperature that accounts for
432 ~25% of the modeled temperature decline between 1 and ~1880 CE. The modeled summer
433 temperature decline is consistent with the earliest kill-date cluster centered on 250-450 CE
434 (Fig. 9C). The modest number of kill-dates between 1 and 250 CE (Fig. 9C) are consistent with
435 the onset of cooling summers 1-250 CE in the model, prior to the main cluster of kill dates
436 beginning at 250 CE.

437 Declining summer temperatures 250-450 CE were followed in the model by 50 years
438 of warmth before a 50-year strongly negative temperature excursion resulting from 536 CE
439 explosive volcanism (Büntgen et al., 2016) and associated positive feedbacks. A record of ice-
440 cap expansion at that time is not present in our kill dates. We presume snowline dropped and
441 ice caps grew at this time, but the short duration and rapid return to a century of relative
442 warmth after the eruption likely resulted in enough melt that evidence of any 536 CE ice-cap
443 expansion is lost.

444 High multi-decadal temperature variability without a trend between 450 and 800 CE
445 is predicted to result in changes in snowline, but because cold summers are brief (2 to 3
446 decades) and followed by warm summers, development of persistent ice caps is unlikely,
447 hence there are no kill dates. However, a strong 100-year cooling trend between 840 and 940
448 CE produced the coldest sustained temperatures of the First Millennium, and aligns with the
449 second main kill-date cluster between 850 and 1000 CE.



450 Modeled Medieval temperatures in our past2k simulation suggest high-magnitude
451 multidecadal variability between 950 and 1200 CE, but without a trend, and at a mean
452 temperature similar to the coldest decades around 400 CE. This is consistent with Medieval
453 times not being warm enough to fully melt ice caps that formed early in the First Millennium.
454 However, the mean Medieval summer temperature is warmer than summers during the 850-
455 1000 CE ice expansion, yet the forty-two sites that have kill-dates between 850 and 1000 CE
456 require ice-cap survival there through Medieval times. The model-data differences through
457 this interval remain unresolved.

458 From 1240 to 1880 CE summer temperatures decline overall in the model, consistent
459 with our kill dates and with the low snowline required by the elevations of sparsely vegetated
460 lowlands (Fig. 2). Finding ~1240 CE kill dates outboard of 1480 CE dates (section 4.1.4),
461 requires a multi-decadal oscillation of ice-cap dimensions (e.g., a ~1240 CE advance, followed
462 by ice recession without all dead moss eroded away, followed by a subsequent advance
463 ~1480 that allowed ice caps to re-cover moss killed in 1240 CE), and to also kill newly
464 colonized moss both inboard and outboard of the 1240 CE sites. This is consistent with
465 modeled summer temperatures exhibiting significant multi-decadal variability, but never
466 warm enough or long enough to melt all ice that expanded ~1240 CE, early in the Little Ice
467 Age. The lack of kill dates younger than 1500 CE suggests it is unlikely there was any century
468 after 1500 CE with average summer temperatures higher than the 1240-1480 CE mean until
469 20th Century warming, which is consistent with modeled summer temperatures (Fig. 10).

470 Modeled summer temperature decreases after Medieval Times are a response to
471 major explosive volcanism ~1240 and ~1440 CE (40 and 50 years, respectively; Sigl et al.,
472 2015). Ten percent of all kill dates (18 of 186 dates; Fig. 9C) have median calibrated ages
473 between 1440 and 1480 suggesting widespread ice expansion then, although the peak at
474 1440 CE in our evaluation of calibration bias (Fig. 8) suggests that the concentration of kill
475 dates is at least in part an artifact related to variations in atmospheric $^{14}\text{CO}_2$ concentrations.
476 Nevertheless, 97 sites with kill dates between 1240 and 1500 CE indicate expansion of ice
477 caps across those two centuries, consistent with large sulfur-rich volcanic eruptions that
478 produce a first-order declining trend in modeled summer temperatures.

479 There is broad agreement between modeled summer temperatures and the temporal
480 distribution of kill-dates, with the three primary clusters of kill dates centered on episodes of
481 centennial-scale declines in past2k modeled summer temperatures. The cluster of kill dates
482 between 1240 and 1480 CE align with the beginning of a 600-year irregular temperature
483 decline in modeled summer temperature, culminating in the coldest century of the Common
484 Era between 1780 and 1880 CE. This cold century is our estimate for the time that permanent
485 ice caps covered the extensive sparsely vegetated regions first noted 70 years ago (Ives,
486 1957), a duration that meets that time required to kill all vegetation. Rapid warming in the
487 past2k model after ~1880 CE is consistent with rapid cryosphere recession that reduced the
488 ice-covered area across the northcentral Baffin Island uplands from ~11,000 km² in ~1880 CE
489 to ~400 km² by 1960 CE, and <100 km² in 2022 CE.

490



491 **5. DISCUSSION**

492

493 5-1 Age of maximum Common Era ice-cap expansion

494 The swaths of sparsely vegetated regions across north-central Baffin Island at elevations well
495 below extant ice caps that define the lowest snowline of the Common Era, have been
496 considered to represent peak cold of the Little Ice Age (Ives, 1962; Andrews et al., 1975; 1976,
497 Williams, 1978; Locke & Locke, 1977), but independent dating of that interval has been
498 elusive. To kill all vegetation requires multi-decadal burial beneath ice. Because the regions
499 that define peak LIA snowline lowering by limited vegetation cover are discontinuous (Fig. 2),
500 more than 100 independent, cold-based ice caps, each a few tens of meters thick, and ranging
501 from ~50 km² to a few hundred km² in area must have mantled the currently sparsely
502 vegetated uplands during a century or more of coldest LIA summers. The spectral character
503 along the outer perimeters of the sparsely vegetated regions (Fig. 2) is mottled, suggesting a
504 dominant “permanent” ice cap over higher hills, and an outer perimeter where permanent
505 snow lay in landscape hollows long enough to kill vegetation, but not long enough to coalesce
506 into the main ice cap.

507 Although sparsely vegetated landscapes define the maximum dimensions of ice caps
508 in the Common Era, vegetation killed by that expansion was vulnerable to efficient removal
509 by wind and water erosion as ice caps receded. In 2005 we visited a “sparsely vegetated”
510 region apparent in remote imagery and found that re-vegetation was already advanced. We
511 sampled a dead willow (*Salix*) stem at 629 m asl, lower than any extant ice cap. The ¹⁴C age
512 of the stem is “modern” (CURL-7929: 1.16 FM), suggesting that vegetation killed by the lowest
513 LIA snowline is rare or absent, and little chance that radiocarbon can resolve when snowline
514 reached its maximum LIA dimensions.

515 Recession of ice caps from regions defined by vegetation contrasts was nearly
516 complete by the middle of the 20th Century when remotely sensed imagery first became
517 available. Because the spectral contrast that defines the sparsely vegetated landscape in
518 imagery from the 1950s is much stronger than in contemporary imagery due to on-going re-
519 vegetation, and because the sparsely vegetated landscapes lack gradients in their spectral
520 contrasts, ice recession from maximum LIA dimensions must have been relatively rapid and
521 continuous.

522 The youngest kill-dates are ~1500 CE, so the timing of maximum snowline lowering
523 must post-date 1500 CE. Having demonstrated that clusters of kill dates align with centuries
524 of simulated cold summers in the past2k simulation, and the past2k simulation aligns with
525 the Dewar Lakes summer temperature record, we use the past2k simulation to estimate the
526 timing of peak snowline lowering defined by sparsely vegetated regions in remote imagery.
527 In the past2k simulation from 1500 to 2000 CE (Fig. 14) an irregular decline in summer
528 temperature reaches lowest values between 1780 and 1880 CE, the coldest century of the
529 Common Era. Subsequently, temperatures rose steadily to the warm decades of the 1930s -
530 1950s. We conclude that the ice caps that killed vegetation apparent in remote imagery,
531 persisted for at least the 100 years of cold summers between 1780 and 1880 CE.



532

533 5.2 Comparing Baffin Island kill-date records with a continuous proxy record of ice-cap
534 expansion in Iceland though the Common Era

535 The composite PDF of 186 kill-dates from 70 ice caps (Fig. 9C) provides a direct record of past
536 ice-cap expansion, with changes in mean summer temperature the primary control on ice-
537 cap dimensions. A major advantage of our dataset is that moss kill-dates require no training
538 sets for their interpretation. Although they are discontinuous records, the discontinuities are
539 often important. Consequently, they differ in significant ways from continuous records of
540 glacier-dimension proxies. To evaluate whether the Baffin kill-date record reflects the
541 evolution of summer temperature for the North Atlantic Arctic, as suggested by the strong
542 correlation with climate model results for those land, we compare the discontinuous moss
543 kill-date record that defines time of glacier expansion on Baffin Island with a continuous,
544 annually resolved Common Era record of glacier dimensions from Iceland, also a part of the
545 North Atlantic Arctic lands included in our model.

546 The Iceland record is derived from annual varve thicknesses in a sediment core from
547 glacial lake Hvítárvatn that drains Langjökull, the second largest ice cap in Iceland. Two
548 primary Langjökull outlet glaciers drain into the lake, and during the Little Ice Age, terminated
549 in the lake. Varve thicknesses are a direct measure of glacier dimensions; as the glacier grows,
550 more erosion occurs, and consequently, thicker annual sediment packets in Hvítárvatn.
551 Because Hvítárvatn freezes in winter, and Langjökull occupies easily eroded basaltic terrain,
552 Hvítárvatn sediment is characterized by high sedimentation rates and consequently
553 measurable annual varve couplets for the past 3000 years or more (Larsen et al., 2011).

554 The Hvítárvatn varve-thickness record over the Common Era is plotted against the
555 moss kill-date record in Fig. 14. Varve thicknesses are low, but easily measured, at the start
556 of the Common Era. There is a slight increase in varve thickness 250-450 CE, coincident with
557 the first cluster of kill-dates. A more prominent spike in varve thickness occurs between 850
558 and 950 CE is coincident with the second Baffin Island kill-date clusters between 850 and 1000
559 CE. The final kill-date cluster (1240-1480 CE) is represented in the Hvítárvatn varve record by
560 increasing varve thicknesses that double between 1240 and 1480 CE. Our estimated age for
561 the lowest Baffin Island snowline (1780-1880 CE) is matched by Langjökull varves remaining
562 relatively thick after 1480 CE until thickening rapidly between 1780 and 1880 CE, when the
563 outlet glaciers terminated in the lake (Larsen et al., 2011). Although historical records confirm
564 Langjökull has been receding since ~1900 CE, Hvítárvatn varves remain thick because
565 Langjökull is much thicker (~600 m) than Baffin Island upland ice caps, so has a longer time
566 constant when responding to large increases in summer temperature.

567 The commonalities between the Hvítárvatn varve thicknesses record as a proxy for
568 Langjökull dimensions and moss kill-dates representing episodes of Baffin Island ice cap
569 expansion, suggests both datasets provide a similar record of regional North Atlantic Arctic
570 summer climate through the Common Era. Most other Arctic Common Era summer
571 temperature reconstructions are pan-Arctic (e.g. McKay and Kaufman, 2014; Werner et al.,
572 2018), and show summer temperature variability through the First Millennium, but without



573 a trend, which differs from our records that show overall summer cooling through the same
574 time interval. The difference is likely because those records are pan-Arctic, whereas our
575 results are limited to the North Atlantic Arctic where the sea ice feedback is stronger, and
576 climate modeling shows pan-arctic spatial gradients in response to natural forcing over the
577 Common Era (Zhong et al., 2018).

578

579 5.3 Evolution of Baffin Island snowline through the Common Era

580 The PDF of all moss kill-dates (Fig. 9C) defines three episodes of ice-cap expansion. We derive
581 an estimate of the corresponding snowline during each expansion from the mean elevation
582 of the lowest 20% of all dated sites for each interval. We define snowline as the lowest
583 elevation that snow or ice persisted long enough to kill all vegetation (multiple decades),
584 sufficient time for snow to turn into ice. During times of lowering snowline, ice margins
585 expand at many elevations. But because the ice caps are cold based and ice velocities are
586 negligible, the lowest ice margins are the closest quantitative estimate of snowline available.
587 We recognize that ice cap margins defined by their kill dates may be smaller than their
588 maximum dimensions due to ice recession before re-burial under a younger ice cap, but those
589 elevations remain the best estimate for the minimum snowline lowering. We estimate
590 snowline at the peak Little Ice Age from the lowest persistent elevation of remnant vegetation
591 trimlines (Fig. 2), and assign an age of 1880 CE to that snowline, as discussed in section 5.1.

592 During the Common Era snowline declined more than 400 m, from an initial elevation
593 above 900 m asl to the sparsely vegetated hills 450 to 500 m asl. To evaluate how a declining
594 snowline elevation translates to the area of permanent ice, we calculate the distribution of
595 area across elevation for the region of low-vegetation cover outlined in Fig. 1. Reconstructed
596 snowline elevations for the three kill-date clusters are mapped on to the area/elevation
597 relationship (Supplemental Fig. 3). To calculate the area of permanent ice-cover at peak-LIA-
598 cold, we measured the area of sparsely vegetated regions (Supplemental Fig. 4). Fig. 15
599 illustrates the highly non-linear relationship between snowline decline and resultant areal
600 extent of permanent ice. Although we lack quantitative snowline data between ice-cap
601 advances, snowline could not have risen much above the preceding low snowline for long or
602 all ice from earlier advances would have melted and no dead vegetation would have been
603 preserved.

604

605 5.4 “Instantaneous glacierization” and the initiation of the Laurentide Ice Sheet

606 The large area of the north-central Baffin Island uplands ice covered at the peak of the Little
607 Ice Age relative to the area currently glacierized (e.g., Fig. 2) led to the concept of
608 “Instantaneous Glacierization” (Ives, 1957; Andrews et al., 1975; Ives et al., 1975) when a
609 modest decline in snowline resulted in a dramatic increase in the area beneath ice caps.
610 Subsequent simulations of conditions leading to the initiation of the Laurentide Ice Sheet
611 from an initial interglacial state (e.g., Andrews and Mahaffy, 1975; Clark et al., 1993; Kleman
612 et al, 2002; Birch et al. 2017; 2018) all show initial snow accumulation on Baffin Island with
613 the albedo feedback providing an important acceleration of ice-sheet growth.



614 The dramatic increase in the area under permanent snow/ice-cover in our field area
615 between 1480 and 1880 CE (Fig. 15), during which time snowline dropped 165 m, from ~665
616 to ~500 m asl, is due to the large area of land between those two elevations (Supplemental
617 Fig. 3). Assuming a standard free air lapse rate of 0.6°C per 100 m, this drop in snowline
618 required a 1°C decrease in mean summer temperature. The direct evidence of “instantaneous
619 glacierization”, constrained by the limits provided by moss kill-dates and climate modeling
620 illustrates how a significant albedo increase may occur following a modest decrease in
621 summer temperature, where the resultant snowline descent results in a dramatic increase in
622 permanently ice-covered lands.

623

624 5.5 Climate forcing that led to 20th Century ice-cap recession

625 The combination of direct evidence and modeled summer temperatures points to rapid
626 recession from maximum Common Era ice-cap coverage across north-central Baffin Island
627 beginning in the late 1800s CE. The past2k model simulates all summers after 1900 CE warmer
628 than the mean summer temperature of the 19th Century, with particularly warm summers
629 between 1920 and 1960 CE (Figs. 14 and 16), similar to Arctic-wide temperatures in multiple
630 climate model simulations with all forcings (Fyfe et al., 2013). The dominant forcings that
631 contribute to warming from 1900 to 1960, by which time remote imagery shows that almost
632 all peak LIA ice caps in the field area (Fig. 2) had melted, include a slight increase in solar
633 irradiance through the early 1900s, significant increases in greenhouse gases (GHG: CO₂, CH₄,
634 and N₂O; Fig. 4), partially compensated by a cooling effect from increased anthropogenic
635 aerosols and land-use change, and a slight decline in Northern Hemisphere summer
636 insolation from orbital terms (e.g., Fyfe et al., 2013).

637 An underlying question is whether the cold century from 1780 to 1880 CE and
638 resultant dramatic increase in ice-covered terrain across north-central Baffin Island was the
639 prelude to a transition into a new ice age, or just an aberrant century that even without
640 anthropogenic trace gas inputs would have returned to warmer summers and ice-cap retreat.
641 The primary impacts on Earth’s planetary energy balance over the past century are the
642 opposing effects of anthropogenic aerosols and greenhouse gases, with modest impacts from
643 solar irradiance and volcanism (Myhre et al. 2013; Zhao et al. 2019).

644 Fyfe et al. (2013) compared pan-Arctic mean annual temperature anomalies over the
645 20th Century in a range of models that included those using only “Natural” forcings (solar
646 irradiance and volcanism) and those using “Historical” forcings (Natural forcings plus
647 greenhouse gas and aerosol forcings). They found that “Natural” simulations resulted in no
648 trend in circum-Arctic mean annual temperatures, whereas “Historical” simulations produced
649 a modest early 20th Century temperature rise, a slight decline in temperature centered on the
650 1960s, and a steady warming thereafter. However, the Fyfe et al. (2013) results cannot be
651 compared in detail to our reconstructed changes in the North Atlantic sector, which behave
652 differently from the pan-Arctic average in paleoclimate models (Zhong et al., 2018). Their
653 conclusions also were for mean annual temperatures, whereas we focus on mean summer
654 temperature, the primary control on glacier mass balance (Koerner, 2005).



655 To test the potential role of anthropogenic forcing in the observed Baffin Island
656 snowline rise after 1880 CE we compare 15-year running means of summer (JJA) temperature
657 over the North Atlantic Arctic lands in a series of CESM1 ensembles beginning in 1850 CE with
658 “Historical” (4 runs) and CESM1 ensembles with only “Natural” forcings (3 runs; Hurrell et al.
659 2013, Meehl et al. 2020, Xu et al 2022) in Fig. 16. The “Historical” and “Natural” ensembles
660 track closely until ~1920 CE, when the “Historical” ensemble continues a long increase in
661 simulated summer temperature, with a temporary reduction in the 1950s and 1960s,
662 whereas the “Natural” forcing simulations fail to show additional increases in summer
663 temperature after 1920. Based on this comparison, it is likely that some rise in snowline in
664 the early 1990s would have occurred without any anthropogenic disturbance in the planetary
665 energy balance, but the significant increase in summer temperatures after 1920 CE seen in
666 both the past2k and “Historical” simulations is primarily a response to anthropogenic
667 impacts. This suggests that without Anthropogenic impacts, Baffin Island ice caps would still
668 be widespread at elevations well below 600 m asl, the lowest elevation ice cap in 1885 CE
669 imagery (Fig. 2).

670

671 6. CONCLUSIONS

672

673 • Small ice caps in the cold, low-relief landscapes of Baffin Island, are frozen to their beds,
674 allowing them to act as preservation agents. Ice cap dimensions are set by summer
675 temperature, with small changes in summer temperature driving significant changes in
676 glacier dimensions. As ice caps expand, they entomb vegetation *in situ*, preserving them until
677 the vegetation is re-exposed when ice caps recede. Radiocarbon dates on moss collected
678 within a few meters of ice-cap margins date times of consistently cold summers resulting in
679 ice-cap expansion through the Common Era, but are restricted to expansions for which
680 subsequent summers never warmed sufficiently and/or long enough to completely melt
681 earlier ice-cap expansions. By inference, summers currently are warmer than any series of
682 multi-decadal summers since the dated ice-cap expansions, placing contemporary warming
683 in a millennial perspective. Kill-dates that define changes in ice cap dimensions are a summer
684 paleo-temperature proxy.

685

686 • None of the 107 kill-dates from plateau ice caps ice-marginal dates within the area inscribed
687 in Fig. 1 pre-date the Common Era. Consequently, if earlier Neoglacial episodes of summer
688 cold resulted in long-lived ice caps across the uplands, subsequent summers were warm
689 enough and/or long enough to completely melt those ice caps before 1 CE.

690

691 • The composite PDF of 186 moss kill-dates collected from seventy ice caps over a region
692 covering more than 50,000 km² yields three multi-century clusters, defining times of
693 widespread ice-cap expansion 250-450 CE, 850-1000 CE, and 1240-1480 CE, continuing
694 without preserved vegetation to a peak snowline lowering between 1780 and 1880 CE,



695 resulting in over $\sim 11,000 \text{ km}^2$ covered by ice caps, across a region where ice caps currently
696 cover $< 100 \text{ km}^2$.

697

698 • Clusters of kill dates defining episodes of multi-decadal cold summers, align with an
699 annually resolved continuous record of ice-cap expansion from Iceland through the Common
700 Era.

701

702 • The annually-resolved record of varve thicknesses in a lake draining Longjökull records the
703 irregular expansion of the ice cap during the same time intervals as Baffin kill dates, with both
704 regions reaching maximum ice dimensions 1780-1880 CE, suggesting that the kill-dates likely
705 reflect the evolution of summer temperature throughout the North Atlantic Arctic.

706

707 • We compare the times of inferred cold summers that led to snowline lowering and ice-cap
708 expansion with the past2k fully coupled climate model for the Common Era with all major
709 forcings. The model simulates decadal averaged summer temperatures that reveal a first-
710 order decline in summer temperatures over the Common Era, consistent with steadily lower
711 snowline estimates derived from the dated ice caps, and centennial intervals of cold summers
712 that align with the clusters of kill-dates. Peak Common Era modeled cold summers between
713 1780 and 1880 led to a snowline decline that dramatically increased the snow-covered
714 regions of the Baffin Island uplands (Instantaneous Glacierization) and brought the Eastern
715 Canadian Arctic perilously close to conditions anticipated at the inception phase of the
716 Laurentide Ice Sheet.

717

718 • Climate modeling over the interval from 1850 CE to present suggests that rapid ice-cap
719 retreat over Baffin Island beginning ~ 1880 CE, but especially after 1920 CE, was driven
720 primarily by anthropogenic forcing. We may never know with certainty whether the dramatic
721 snowline decline, and resultant aerial increase in permanently snow-covered lands in Arctic
722 Canada at the peak of the Little Ice Age heralded the onset of the next Northern Hemisphere
723 ice age, only to be reversed by the increase in greenhouse gases and other forcing agents
724 related to the Industrial Revolution. Summer insolation across the Arctic was near its orbitally
725 driven minimum at the peak of the Little Ice Age, and will continue to decrease slightly
726 through the 21st Century. The strong positive correlation between Arctic summer
727 temperatures and summer insolation (Kaufman et al, 2009) suggests that only the additional
728 anthropogenic forcings since ~ 1850 CE reversed the natural transition into a new ice age.

729

730 **FIGURES**

731



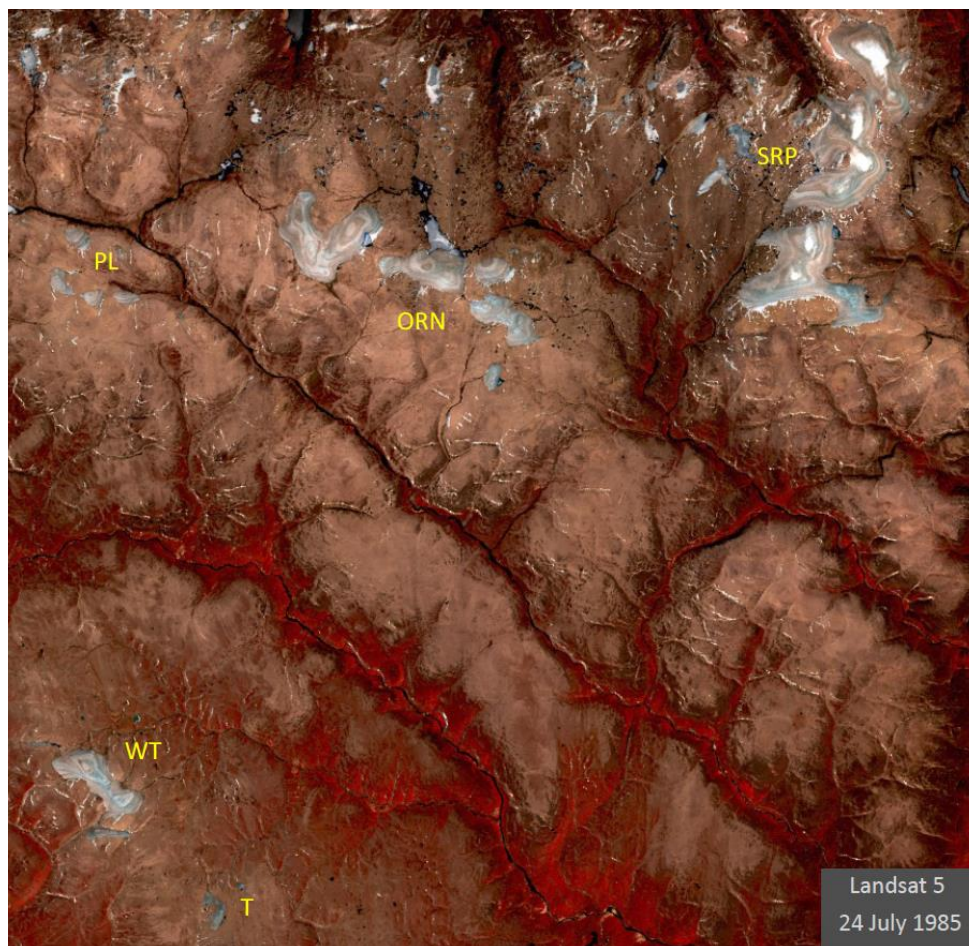
732

733 Figure 1 Field area, northern Baffin Island. Solid line defines regions for which the area-
734 elevation relation is quantified in Supplemental Figure 1 and used to reconstruct the area
735 covered by descending snowlines (Fig. 15). Dotted white square is the area covered by Fig. 2.
736 Encircled dots show locations of all 186 moss kill-dates (some dots include multiple samples).
737 A portion of the Barnes Ice Cap is in lower right corner. Basemap © Google Earth.

738

739

740



741
742

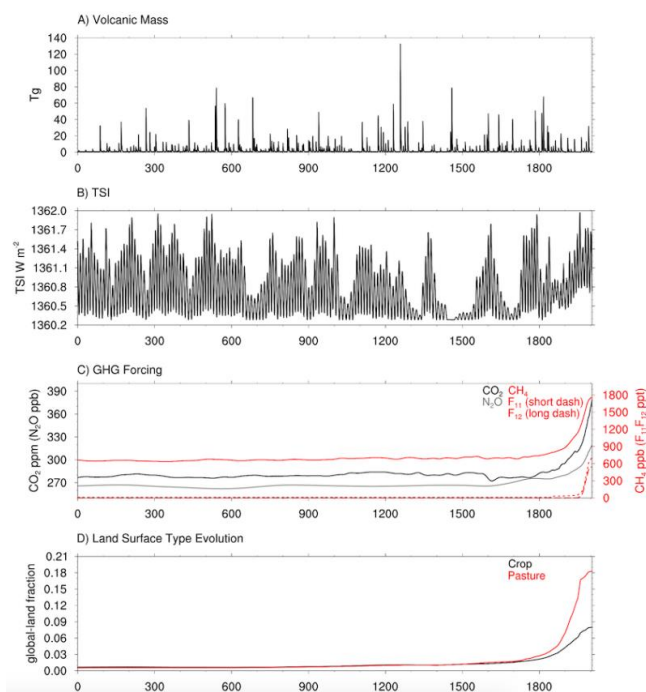
743 Figure 2 Landsat 5 image from summer 1985, color-enhanced to maximize the spectral
744 contrast that highlights lighter-toned regions that are sparsely vegetated. Those regions were
745 beneath ice caps for a century or more during peak summer cold of the Little Ice Age. Labels
746 are for the Serpens (SRP) and Orion (ORN) ice-cap complexes, and White Tiger (WT) and Tiger
747 (T) ice caps, and Pleiades ice-cap cluster (PL). Location of image shown in Figure 1-1.

748
749
750
751
752
753
754
755



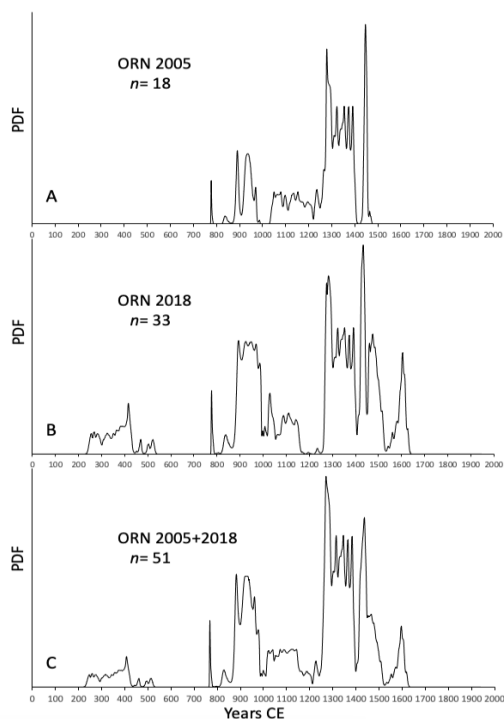
756

757 Figure 3 Delicately perched boulder left by the receding Laurentide Ice Sheet that has recently
758 emerged by down-wasting of the local ice cap in background. The preservation of such
759 delicate features demonstrates the lack of internal deformation in the cold-based, ice caps
760 that mantle the low relief hills of the Baffin Island uplands. Photo by GHM.



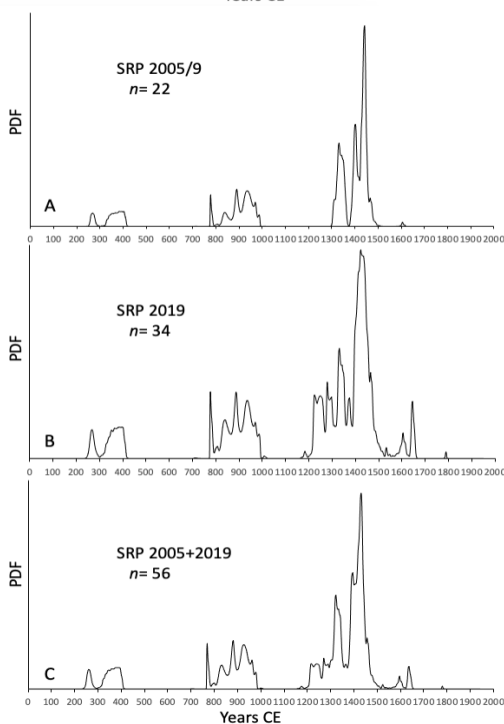
761

762 Figure 4 Forcing used for the past2k climate model discussed in the text. A) Mass of sulfuric
763 acid injected into the stratosphere by explosive volcanism in teragrams. B) Total solar
764 irradiance (TSI) in watts /m². C) Concentrations of anthropogenic greenhouse gasses released
765 through the Common Era. D) Anthropogenic changes in global land cover through the
766 development of crop (upper line) and pasture (lower line) through the Common Era.



767

Figure 5 Probability density functions (PDF) for calibrated radiocarbon dates on dead moss collected around the margins of the Orion Ice Complex (ORN, Fig. 2-2), which consists of several adjacent ice caps. (A) The PDF of 18 samples collected in 2005. (B) The PDF of 33 samples collected in 2018 mirrors the distribution from 2005, except for the addition of early First Millennium samples in the latter group, that reflect a buried ice cap now emerging from beneath a younger ice cap that grew on top of it. (C) PDF of all dates from ORN from all years



768

Figure 6 Probability density functions (PDF) for calibrated radiocarbon dates on dead moss collected around the margins of the Serpens Ice Complex (SRP, Fig. 2-2), which consists of three adjacent ice caps. (A) The PDF of 22 samples collected in 2005 (3 from 2009). (B) The PDF from 34 samples collected in 2019. (C) The composite PDF for all kill dates from SRP form three discrete age clusters that exhibit little change between collection dates, despite significant (~250 m) ice-margin recession.

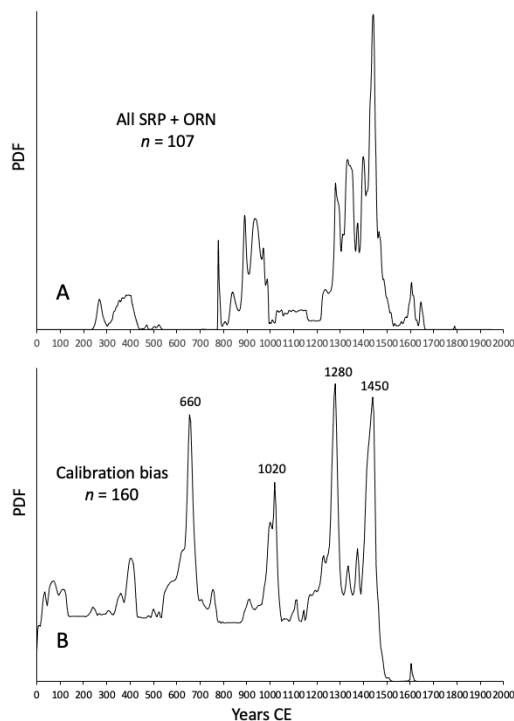


Figure 7 A comparison between probability density functions (PDF) for all calibrated radiocarbon dates on dead moss collected around the margins of ORN (A) and SRP (B) ice complexes (Fig. 2-2) showing the similarities between the two data sets. The composite PDF for the 107 moss kill-dates from both ice complexes (C) defines tightly clustered episodes of ice cap expansion through the Common Era 250-400 CE, 850-1000 CE, and between ~1240 and 1480 CE.

769

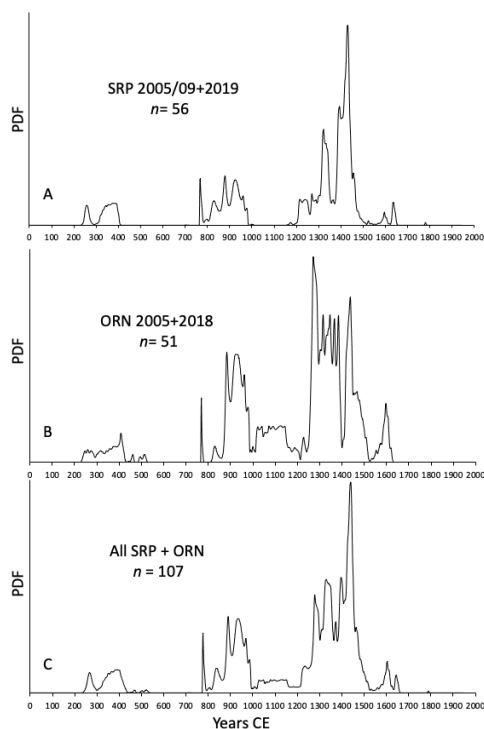
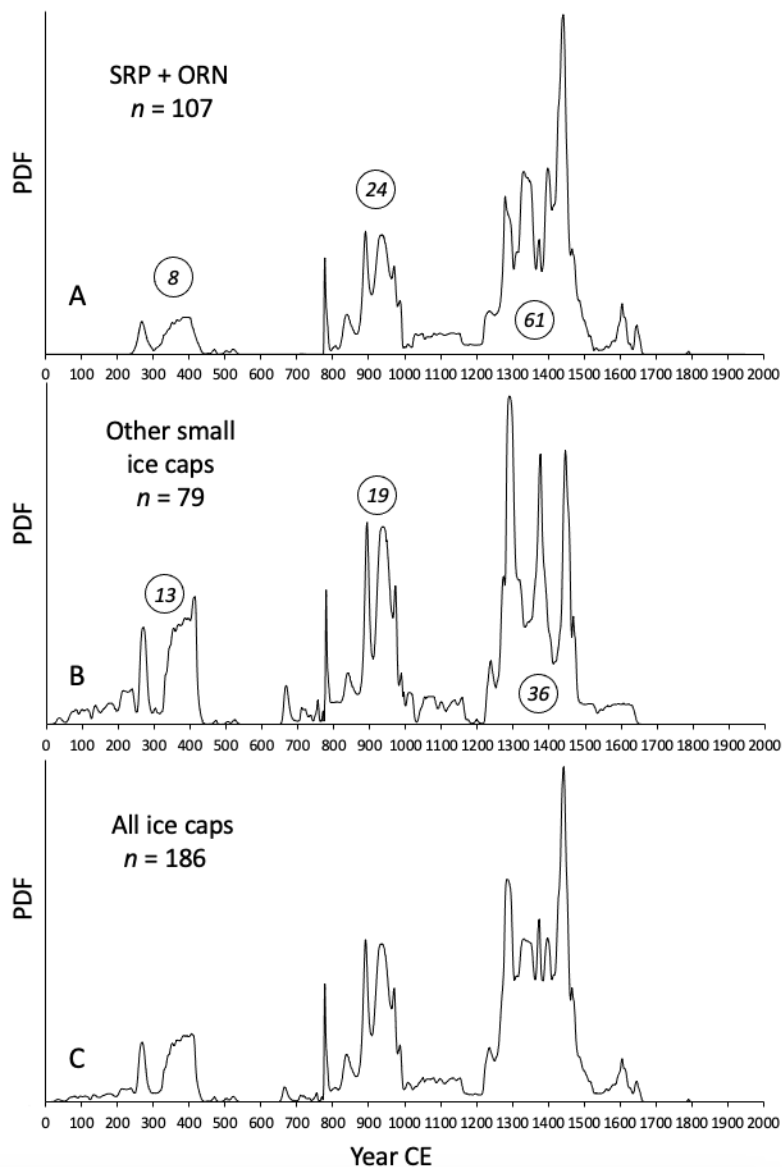


Figure 8 The composite kill-date PDF for SRP+ORN (top panel) compared to the PDF of 160 randomly generated ^{14}C ages between 1 and 1500 CE (bottom panel) to test whether changes in atmospheric $^{14}\text{CO}_2$ concentrations and resultant bias in the calibrated ages contributed to the clustering of kill dates in the SRP and ORN composite PDFs. Neither of the earlier calibration peaks (660 and 1020 CE) have any power in the SRP or ORN PDF. However, both the 1280 and 1450 CE peaks coincide peaks in the SRP and ORN PDFs, suggesting that at least some of the magnitude of those two spikes, especially the 1450 CE spike, is due to natural variations in atmospheric $^{14}\text{CO}_2$ concentrations rather than an abundance of ice-expansion. However, the calibration artifact does not affect the conclusion that ice caps were advancing at about those times.

770

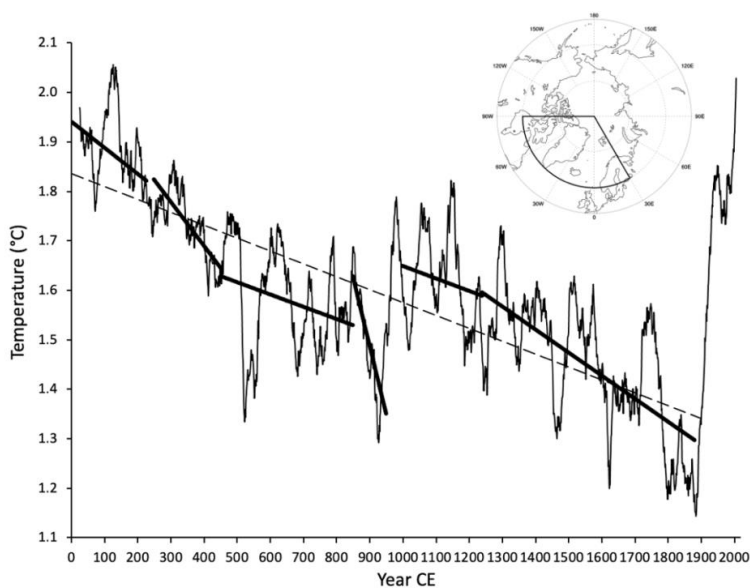


771



772

773 Figure 9 The PDF for all moss kill-dates from SRP+ORN (A) and the PDF for all kill-dates from the margins of all
774 other small ice caps (B) are composited in Panel C. Moss kill-dates that make up Panel B are from 62 different
775 ice caps (Fig. 1-1), all within 250 km of the SRP and ORN ice complexes. The number of dates in each of the
776 clusters is given as a circled number. The similarities between PDFs in Panels A and B is striking, suggesting ice-
777 cap response to climate forcing over the Common Era was uniform across northern Baffin Island, and lends
778 confidence to a comparison of ice-cap response and modeled climate forcing. Location data, Lab-ID, ¹⁴C ages
779 and the PDF for each sample in Panel C are available in Supplemental Table S-1. The spike at ~780 CE is a
780 calibration artifact. The height of the spikes at 1280 and 1450 CE may also be amplified by natural biases in the
781 calibration process.



782

783 Figure 10 Fifty-year running means of modeled annual summer (J, J, A) temperature over land areas
784 north of 60° and between 30° and 90° west latitude between years 1 and 2005 CE in our CESM past2k
785 simulation. Dashed black line is a least-squares linear regression for the data between 1 and 1890 CE,
786 showing a first order trend of declining summer temperature through the Common Era. Solid lines are
787 least-squares linear regressions through times defined by clusters of kill dates, and the times between
788 kill-date clusters in Figure 9C. The regressions allow a direct comparison of summer temperature
789 trends and relative magnitudes for intervals characterized by widespread ice-cap expansion
790 (predicted cold summers), and intervals lacking evidence of sustained ice-cap expansion (predicted
791 mild summers). The time-intervals defined by these trends can be compared to the reconstructed
792 snowline elevations through the Common Era (Fig. 15).

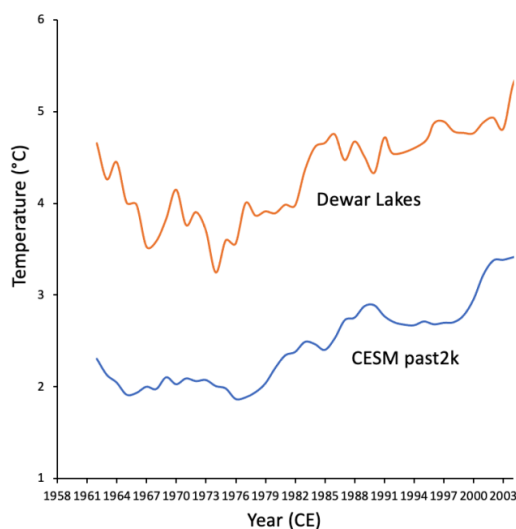


Figure 11 10-year running mean for JJA temperature measured daily at Dewar Lakes since 1958 (upper line) and 5-year running means of simulated JJA 2-m temperature over land north of 60°N and between 30°E and 90°W in our CESM past2k model run (lower line). Dewar Lakes temperature are more strongly smoothed because site-specific records have greater variability than past2k, which is averaged over a large area that naturally smooths the data.

793

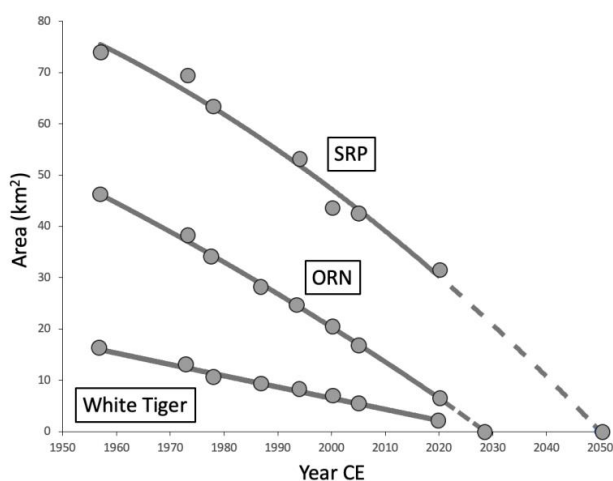


Figure 12 The area of three named caps in Figure 2, between 1957 and 2020. Serpens Ice Complex (SRP; 3 ice caps), Orion Ice Complex (ORN; 6 ice caps, 4 remaining in 2020 CE), and White Tiger (WT, one ice cap). All three show decreased recession rates between 1957 and 1972 CE, consistent with cold summers recorded at Dewar Lakes over the decade between 1958 and mid 1970s CE, followed by steady, or increasing rates of mass loss after 1972,. Areas are derived from vertical aerial photography from 1957 CE and satellite imagery subsequently. Updated from Anderson et al. (2008).

794

795

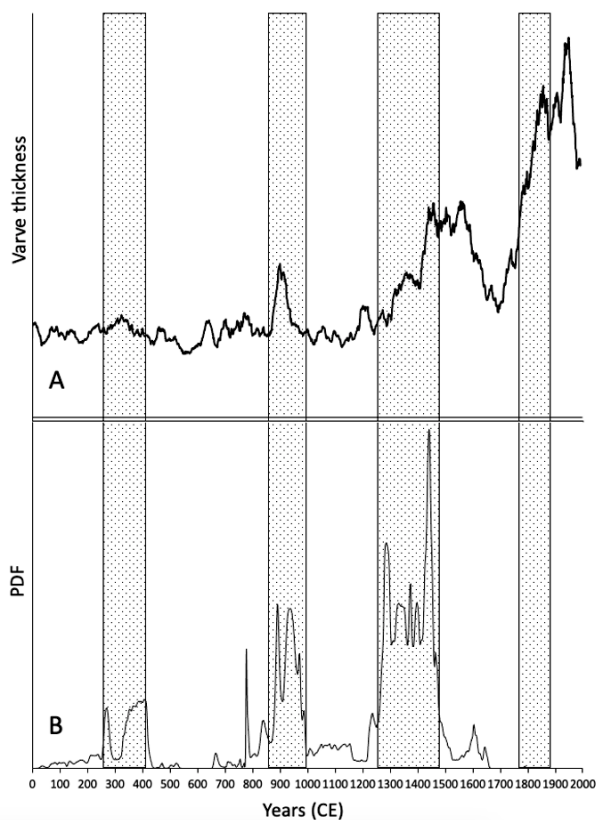


Figure 13 Comparison of 15-year running means of annual varve thickness in glacial lake Hvítárvatn (A), a proxy for the size of Langjökull, second largest glacier in Iceland, and moss kill-date clusters from Baffin Island (B). Stippled boxes show the close correspondence between growth of Langjökull and expansion of Baffin Island ice caps. The varves also confirm that Langjökull attained its greatest dimension in the late 1800s CE, the same time Baffin Island snowline was at its lowest of the Common Era. That close correspondence suggests Baffin kill-dates and Hvítárvatn varves provide a North Atlantic Arctic temperature history for the Common Era.

796

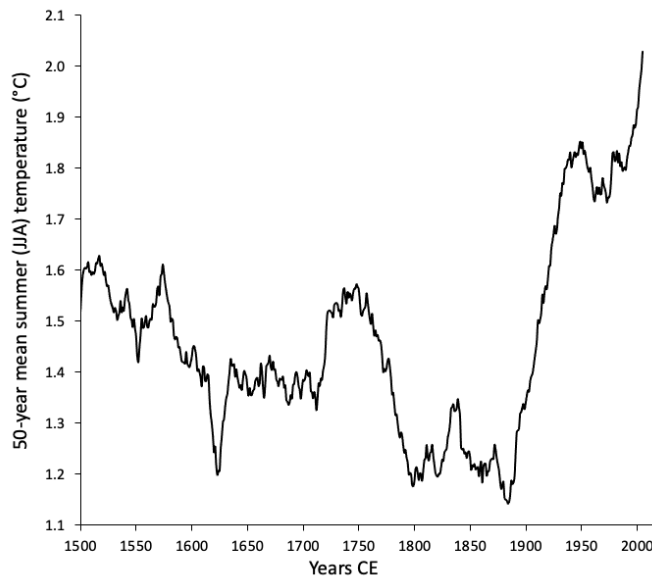
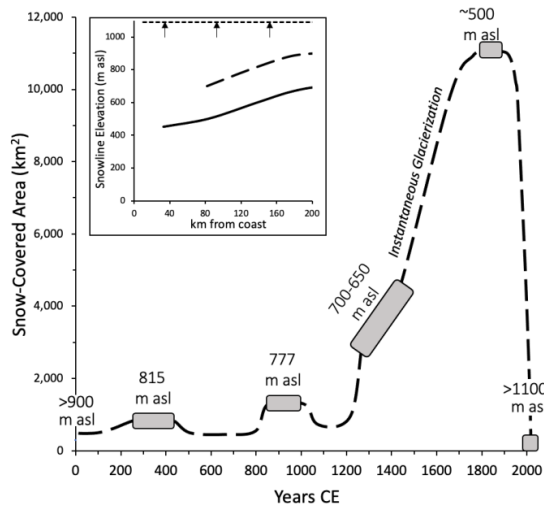


Figure 14 Fifty-year running means of summer (JJA) temperatures in our past2k simulation illustrating the strong trend in declining summer temperatures after 1500 CE (our youngest kill dates), the peak cold century (1780-1880 CE) and rapid summer temperature rise after 1900 CE.

797



798

799

800

801

802

803

804

805

806

807

808

Figure 15 Changes in ice-covered area through the Common Era within our prescribed field area (Fig. 1). Episodes of ice-cap expansion derived from moss kill-dates (Fig. 9C); square boxes) and their associated snowline elevation listed above each box, are plotted against the ice-covered area based on the area-elevation relation within the field area as shown in Supplemental Figure 3. The area covered by ice caps 1780-1880 CE is the summed areas defined by vegetation trim lines (Supplemental Figure 4), with the age derived from the past2k modeled temperatures (section 5.2). Inset show the snowline elevations through our field area for 1880 CE (solid line), 1960 CE (dashed line) and snowline everywhere is above 2020 CE (dotted line), The dramatic increase in area of permanently covered ice as snowline descended through the Little Ice Age was originally postulated by Ives (1957) to result in “instantaneous glacierization” due to the significant albedo increase that might lead to the onset of an ice age (Andrews and Mahaffy, 1975; Clark et al., 1993; Birch et al., 2017).



809 **7. SUPPLEMENTAL DOCUMENTS**

810

811 **8. AUTHOR CONTRIBUTIONS**

812 GHM conceived the project. GHM, SLP, SJL, JPB, JHR, HB, MR collected samples, AJ and YZ
813 were responsible for climate modeling with assistance from ÁG and GHM. SJL and JRS were
814 responsible for the ¹⁴C dating. GHM wrote the manuscript with help from all authors.

815

816 **9. COMPETING INTERESTS:** The authors declare that they have no conflict of interest.

817

818 **10. ACKNOWLEDGEMENTS**

819 We gratefully acknowledge the Qikiqtaani Inuit and the Government of Nunavut for
820 permission to access their land through research permits issued by the Nunavut Research
821 Institute. We thank the Inuit of Qikiqtarjuaq for friendships, advice, and field guides over
822 many decades, and members of the Nunavut Research Institute for assistance in Iqaluit.
823 Battelle ARO and Polar Continental Shelf Program, Government of Canada, provided logistical
824 support. We thank the INSTAAR Laboratory for AMS Radiocarbon Preparation and Analysis
825 for sample preparation, and The Keck Carbon Cycle AMS Laboratory University of California,
826 Irvine, for radiocarbon measurements. Digital Globe acquired high-resolution imagery for
827 some of our ice caps through a cooperative agreement with the US-NSF. The field collections
828 and dating were supported by the US National Science Foundation through grants 0454662,
829 0909347, 1204096, 1418040, 1556627, and 1737715. Past2k climate modeling was funded
830 jointly by a Grant of Excellence (141573-053) from the Icelandic Research Center (RANNIS)
831 and the US National Science Foundation 1204096. The CESM project is supported by the
832 National Science Foundation and the Office of Science (BER) of the U.S. Department of
833 Energy. We acknowledge supercomputing resources for all used CESM simulations, provided
834 by NSF/CISL/Yellowstone and the Oak Ridge Leadership Computing Facility supported by the
835 Office of Science (BER) of the Department of Energy under Contract DE-AC05-00OR22725.

836 The past2k model output is available
837 at https://www.earthsystemgrid.org/dataset/ucar.cgd.cesm4.past2k_transient.html while
838 the natural forcing CESM simulations (b.e10.B20NATC5CN.f09_g16) are available here
839 ([https://portal.nersc.gov/archive/home/c/ccsm/www/CESM-CAM5-SF-
No/atm/proc/tseries/monthly/TREFHT](https://portal.nersc.gov/archive/home/c/ccsm/www/CESM-CAM5-SF-No/atm/proc/tseries/monthly/TREFHT))

841 and the full forcing simulations (b.e10.B20TRC5CN.f09_g16) are available
842 at [https://www.earthsystemgrid.org/search.html?Project=CMIP5&q&page=1&rpp=20&Mo-
del=CESM1-CAM5&Experiment=historical](https://www.earthsystemgrid.org/search.html?Project=CMIP5&q&page=1&rpp=20&Model=CESM1-CAM5&Experiment=historical).

844 Dewar Lake climate data are available from [https://www.canada.ca/en/environment-
climate-change/](https://www.canada.ca/en/environment-climate-change/).

846

847



848 11. REFERENCES

849

Literature Cited

- 850 Anderson, R.K., Miller, G.H., Briner, J.P., Lifton, N.A., DeVogel, S.B., 2008. A millennial perspective on Arctic
851 warming from ^{14}C in quartz and plants emerging from beneath ice caps. 2008. *Geophysical Research Letters*
852 35 (1): L01502, <https://doi.org/10.1029/2007GL032057>.
- 853 Andrews, J T; Davis, P T, Wright, C., 1976. Little Ice Age permanent snowcover in the Eastern Canadian Arctic:
854 Extent mapper from LandSat-1 satellite imagery. *Geog. Annaler*, 58A: 71-81.
- 855 Andrews, J T, and M A W Mahaffy. 1976. "Growth Rate of the Laurentide Ice Sheet and Sea Level Lowering (with
856 Emphasis on the 115,000 BP Sea Level Low)." *Quaternary Research* 6: 167–83.
- 857 Birch, Leah, Timothy Cronin, and Eli Tziperman. 2018. "The Role of Regional Feedbacks in Glacial Inception on
858 Baffin Island: The Interaction of Ice Flow and Meteorology." *Climate of the Past* 14 (10): 1441–62.
859 <https://doi.org/10.5194/cp-14-1441-2018>.
- 860 Birch, Leah, Timothy Cronin, and Eli Tziperman. 2017. "Glacial Inception on Baffin Island: The Role of Insolation,
861 Meteorology, and Topography." *Journal of Climate* 30 (11): 4047–64. <https://doi.org/10.1175/JCLI-D-16-0576.1>.
- 863 Briner, J P, P T Davis, and G H Miller. 2009. "Latest Pleistocene and Holocene Glaciation of Baffin Island, Arctic
864 Canada: Key Patterns and Chronologies." *Quaternary Science Reviews* 28: 2075–2087.
- 865 Briner, J.P., N. Michelutti, D.R. Francis, G.H. Miller, Y. Axford, M.J. Wooller, A.P. Wolfe, Y. Axford. and A.P. Wolfe.
866 2006. "A Multi-Proxy Lacustrine Record of Holocene Climate Change on Northeastern Baffin Island, Arctic
867 Canada." *Quaternary Research* 65 (3): 431–42. <https://doi.org/10.1016/j.yqres.2005.10.005>.
- 868 Briner, Jason P., Nicholas P. McKay, Yarrow Axford, Ole Bennike, Raymond S. Bradley, Anne de Vernal, David
869 Fisher, et al. 2016. "Holocene Climate Change in Arctic Canada and Greenland." *Quaternary Science*
870 *Reviews* 147: 340–64. <https://doi.org/10.1016/j.quascirev.2016.02.010>.
- 871 Büntgen, Ulf, Vladimir S. Myglan, Fredrik Charpentier Ljungqvist, Michael McCormick, Nicola Di Cosmo, Michael
872 Sigl, Johann Jungclauss, et al. 2016. "Cooling and Societal Change during the Late Antique Little Ice Age
873 from 536 to around 660 AD." *Nature Geoscience* 9 (3): 231–36. <https://doi.org/10.1038/ngeo2652>.
- 874 Calkin, P. E., and J. M. Ellis. 1981. "A Cirque-Glacier Chronology Based on Emergent Lichens and Mosses." *Journal*
875 *of Glaciology* 27 (97): 511–15. <https://doi.org/10.1017/S0022143000011576>.
- 876 Clark, P. U., J. J. Clague, B. B. Curry, A. Dreimanis, S. R. Hicock, G. H. Miller, G. W. Berger, et al. 1993. "Initiation
877 and Development of the Laurentide and Cordilleran Ice Sheets Following the Last Interglaciation."
878 *Quaternary Science Reviews* 12 (2): 79–114. [https://doi.org/10.1016/0277-3791\(93\)90011-A](https://doi.org/10.1016/0277-3791(93)90011-A).
- 879 Clark, Peter U. 1994. "Unstable Behavior of the Laurentide Ice Sheet over Deforming Sediment and Its
880 Implications for Climate Change." *Quaternary Research*. <https://doi.org/10.1006/qres.1994.1002>.
- 881 Crump, S.E., L.S. Anderson, G.H. Miller, and R.S. Anderson. 2017. "Interpreting Exposure Ages from Ice-Cored
882 Moraines: A Neoglacial Case Study on Baffin Island, Arctic Canada." *Journal of Quaternary Science*.
883 <https://doi.org/10.1002/jqs.2979>.
- 884 Deser, Clara, Adam S. Phillips, Isla R. Simpson, Nan Rosenbloom, Dani Coleman, Flavio Lehner, Angeline G.
885 Pendergrass, Pedro Dinezio, and Samantha Stevenson. 2020. "Isolating the Evolving Contributions of



- 886 Anthropogenic Aerosols and Greenhouse Gases: A New CESM1 Large Ensemble Community Resource.”
887 *Journal of Climate* 33 (18): 7835–58. <https://doi.org/10.1175/JCLI-D-20-0123.1>.
- 888 Dyke, Arthur S. 2004. “An Outline of North American Deglaciation with Emphasis on Central and Northern
889 Canada.” *Developments in Quaternary Science* 2 (PART B): 373–424. [https://doi.org/10.1016/S1571-](https://doi.org/10.1016/S1571-0866(04)80209-4)
890 0866(04)80209-4.
- 891 Francis, Jennifer A., Stephen J. Vavrus, and Judah Cohen. 2017. “Amplified Arctic Warming and Mid-Latitude
892 Weather: New Perspectives on Emerging Connections.” *Wiley Interdisciplinary Reviews: Climate Change* 8
893 (5): 1–11. <https://doi.org/10.1002/wcc.474>.
- 894 Fyfe, John C., Knut Von Salzen, Nathan P. Gillett, Vivek K. Arora, Gregory M. Flato, and Joseph R. McConnell.
895 2013. “One Hundred Years of Arctic Surface Temperature Variation Due to Anthropogenic Influence.”
896 *Scientific Reports* 3: 1–7. <https://doi.org/10.1038/srep02645>.
- 897 Gardner, A., G. Moholdt, A. Arendt, and B. Wouters. 2012. “Accelerated Contributions of Canada’s Baffin and
898 Bylot Island Glaciers to Sea Level Rise over the Past Half Century.” *Cryosphere* 6 (5): 1103–25.
899 <https://doi.org/10.5194/tc-6-1103-2012>.
- 900 Goldewijk, K., Beusen, A., Van Drecht, G. and De Vos, M., 2011. The HYDE 3.1 spatially explicit database of
901 human-induced global land-use change over the past 12,000 years. *Global Ecology and*
902 *Biogeography*, 20(1), pp.73-86. <https://doi.org/10.1111/j.1466-8238.2010.00587.x>
- 903 Groff, Dulcinea V., David W. Beilman, Zicheng Yu, Derek Ford, and Zhengyu Xia. 2023. “Kill Dates from Re-
904 Exposed Black Mosses Constrain Past Glacier Advances in the Northern Antarctic Peninsula.” *Geology* 51
905 (3): 257–61. <https://doi.org/10.1130/g50314.1>.
- 906 Harning, David J., Áslaug Geirsdóttir, Gifford H. Miller, and Leif Anderson. 2016. “Episodic Expansion of
907 Drangajökull, Vestfirðir, Iceland, over the Last 3 Ka Culminating in Its Maximum Dimension during the Little
908 Ice Age.” *Quaternary Science Reviews* 152: 118–31. <https://doi.org/10.1016/j.quascirev.2016.10.001>.
- 909 Hugonnet, R., McNabb, R., Berthier, E. et al. Accelerated global glacier mass loss in the early twenty-first
910 century. *Nature* 592, 726–731 (2021). <https://doi.org/10.1038/s41586-021-03436-z>
- 911 Hurrell, James W., M. M. Holland, P. R. Gent, S. Ghan, Jennifer E. Kay, P. J. Kushner, J. F. Lamarque, et al. 2013.
912 “The Community Earth System Model: A Framework for Collaborative Research.” *Bulletin of the American*
913 *Meteorological Society* 94 (9): 1339–60. <https://doi.org/10.1175/BAMS-D-12-00121.1>.
- 914 Ives, J D. 1957. Glaciation of the Torngat Mountains, Northern Labrador. *Arctic* 10: 67–87.
- 915 Ives, JD. 1962. Indications of recent extensive glacierization in north-central Baffin Island, NWT. *J. Glaciology* ,4:
916 197-205 <https://doi.org/10.3189/S0022143000027398>
- 917 Ives, J D, J T Andrews, and R G Barry. 1975. “Growth and Decay of the Laurentide Ice Sheet and Comparisons
918 with Fenno-Scandinavia.” *Die Naturwissenschaften* 62: 118–25.
- 919 Jungclaus, Johann H., Edouard Bard, Mélanie Baroni, Pascale Braconnot, Jian Cao, Louise P. Chini, Tania Egorova,
920 et al. 2017. “The PMIP4 Contribution to CMIP6 - Part 3: The Last Millennium, Scientific Objective, and
921 Experimental Design for the PMIP4 Past1000 Simulations.” *Geoscientific Model Development* 10 (11):
922 4005–33. <https://doi.org/10.5194/gmd-10-4005-2017>.
- 923 Kleman, J, J Fastook, and A P Stroeven. 2002. “Geologically and Geomorphologically Constrained Numerical
924 Model of Laurentide Ice Sheet Inception and Build-Up.” *Quaternary International* 95–6: 87–98.



- 925 Koerner, Roy M. 2005. "Mass Balance of Glaciers in the Queen Elizabeth Islands, Nunavut, Canada." *Annals of*
926 *Glaciology* 42 : 417–23. <https://doi.org/10.3189/172756405781813122>.
- 927 Locke, C.W. and Locke, W.L.III. 1991. Little Ice Age Snow-Cover Extent and Paleoglaciation Thresholds: North-
928 Central Baffin Island, N.W.T., Canada *Arctic & Alpine Research* 23 (4): 436–
929 43. <http://www.istoir.org/stable/1550544>.
- 930 Larsen, D.J., G.H. Miller, Á. Geirsdóttir, and T. Thordarson. 2011. "A 3000-Year Varved Record of Glacier Activity
931 and Climate Change from the Proglacial Lake Hvítárvatn, Iceland." *Quaternary Science Reviews* 30 (19–20).
932 <https://doi.org/10.1016/j.quascirev.2011.05.026>.
- 933 Lecavalier, Benoit S., David A. Fisher, Glenn A. Milne, Bo M. Vinther, Lev Tarasov, Philippe Huybrechts, Denis
934 Lacelle, et al. 2017. "High Arctic Holocene Temperature Record from the Agassiz Ice Cap and Greenland
935 Ice Sheet Evolution." *Proceedings of the National Academy of Sciences of the United States of America* 114
936 (23): 5952–57. <https://doi.org/10.1073/pnas.1616287114>.
- 937 Lenaerts, Jan T.M., Jan H. Van Angelen, Michiel R. Van Den Broeke, Alex S. Gardner, Bert Wouters, and Erik Van
938 Meijgaard. 2013. "Irreversible Mass Loss of Canadian Arctic Archipelago Glaciers." *Geophysical Research*
939 *Letters* 40 (5): 870–74. <https://doi.org/10.1002/grl.50214>.
- 940 Lowell, Thomas V., Brenda L. Hall, Meredith A. Kelly, Ole Bennike, Amanda R. Lusas, William Honsaker, Colby A.
941 Smith, Laura B. Levy, Scott Travis, and George H. Denton. 2013. "Late Holocene Expansion of Istorvet Ice
942 Cap, Liverpool Land, East Greenland." *Quaternary Science Reviews* 63: 128–40.
943 <https://doi.org/10.1016/j.quascirev.2012.11.012>.
- 944 MacFarling Meure, C., D. Etheridge, C. Trudinger, P. Steele, R. Langenfelds, T. Van Ommen, A. Smith, and J. Elkins.
945 2006. "Law Dome CO₂, CH₄ and N₂O Ice Core Records Extended to 2000 Years BP." *Geophysical Research*
946 *Letters* 33 (14): 2000–2003. <https://doi.org/10.1029/2006GL026152>.
- 947 Margreth, A., Dyke, A.S., Gosse, J.C., Telka, A.M. 2014. "Neoglacial Ice Expansion and Late Holocene Cold-Based
948 Ice Cap Dynamics on Cumberland Peninsula, Baffin Island, Arctic Canada." *Quaternary Science Reviews* 91:
949 242–56. <https://doi.org/10.1016/j.quascirev.2014.02.005>.
- 950 Medford, Aaron K., Brenda L. Hall, Thomas V. Lowell, Meredith A. Kelly, Laura B. Levy, Paul S. Wilcox, and Yarrow
951 Axford. 2021. "Holocene Glacial History of Renland Ice Cap, East Greenland, Reconstructed from Lake
952 Sediments." *Quaternary Science Reviews* 258: 106883. <https://doi.org/10.1016/j.quascirev.2021.106883>.
- 953 Medrzycka, Dorota, Luke Copland, and Brice Noël. 2023. "Rapid Demise and Committed Loss of Bowman Glacier,
954 Northern Ellesmere Island, Arctic Canada." *Journal of Glaciology*, 1–14.
955 <https://doi.org/10.1017/jog.2022.119>.
- 956 Meehl, G.A., A. Hu, F. Castruccio, M.H. England, S.C. Bates, G. Donabasoglu, S. McGregor, J.M. Arblaster, S.-P.
957 Xie, and N. Rosenbloom, 2020: Atlantic and Pacific tropics connected by mutually interactive decadal-
958 timescale processes, *Nature Geo.*, doi:10.1038/s41561-020-00669-x.
- 959 Miller, G.H. 1973. Late Quaternary Glacial and Climatic History of Northern Cumberland Peninsula, Baffin Island,
960 N.W.T., Canada. *Quaternary Research* 3: 561-583
- 961 Miller, G H, A Geirsdottir, Y Zhong, D J Larsen, B Otto-Bliesner, M M Holland, D A Bailey, et al. 2012. "Abrupt
962 Onset of the Little Ice Age Triggered by Volcanism and Sustained by Sea-Ice/Ocean Feedbacks."
963 *Geophysical Research Letters* 39. <https://doi.org/10.1029/2011GL050168>.



- 964 Miller, G.H., R.B. Alley, J. Brigham-Grette, J.J. Fitzpatrick, L. Polyak, M.C. Serreze, and J.W.C. White. 2010. "Arctic
965 Amplification: Can the Past Constrain the Future?" *Quaternary Science Reviews* 29 (15–16): 1779–90.
966 <https://doi.org/10.1016/j.quascirev.2010.02.008>.
- 967 Miller, G.H., A.P. Wolfe, J.P. Briner, P.E. Sauer, and A. Nesje. 2005. "Holocene Glaciation and Climate Evolution
968 of Baffin Island, Arctic Canada." *Quaternary Science Reviews* 24 (14–15): 1703–21.
969 <https://doi.org/10.1016/j.quascirev.2004.06.021>.
- 970 Miller, G.H., J.Y. Landvik, S.J. Lehman, and J.R. Southon. 2017. "Episodic Neoglacial Snowline Descent and Glacier
971 Expansion on Svalbard Reconstructed from the ¹⁴C Ages of Ice-Entombed Plants." *Quaternary Science
972 Reviews* 155. <https://doi.org/10.1016/j.quascirev.2016.10.023>.
- 973 Miller, Gifford H., Scott J. Lehman, Kurt A. Refsnider, John R. Southon, and Yafang Zhong. 2013. "Unprecedented
974 Recent Summer Warmth in Arctic Canada." *Geophysical Research Letters* 40 (21): 5745–51.
975 <https://doi.org/10.1002/2013GL057188>.
- 976 Moore, J.J., K A Kughen, G.H. Miller, J.T. Overpeck. 2001. Little Ice Age Recorded in Summer Temperature
977 Reconstruction from Varved Sediments of Donard Lake, Baffin Island, Canada. *Journal of Paleolimnology*
978 25 (4): 503–17. <https://doi.org/10.1023/A:1011181301514>.
- 979 Myhre, G., B. H. Samset, M. Schulz, Y. Balkanski, S. Bauer, T. K. Berntsen, H. Bian, et al. 2013. Radiative Forcing
980 of the Direct Aerosol Effect from AeroCom Phase II Simulations. *Atmospheric Chemistry and Physics* 13 (4):
981 1853–77. <https://doi.org/10.5194/acp-13-1853-2013>.
- 982 Noël, Brice, Willem Jan van de Berg, Stef Lhermitte, Bert Wouters, Nicole Schaffer, and Michiel R. van den
983 Broeke. 2018. "Six Decades of Glacial Mass Loss in the Canadian Arctic Archipelago." *Journal of Geophysical
984 Research: Earth Surface* 123 (6): 1430–49. <https://doi.org/10.1029/2017JF004304>.
- 985 Otto-Bliesner, Bette L., Esther C. Brady, John Fasullo, Alexandra Jahn, Laura Landrum, Samantha Stevenson, Nan
986 Rosenbloom, Andrew Mai, and Gary Strand. 2016. Climate Variability and Change since 850 Ce an
987 Ensemble Approach with the Community Earth System Model. *Bulletin of the American Meteorological
988 Society* 97 (5): 787–801. <https://doi.org/10.1175/BAMS-D-14-00233.1>.
- 989 Pendleton, S.L., G.H. Miller, R.A. Anderson, S.E. Crump, Y. Zhong, A. Jahn, and Á. Geirsdottir. 2017. "Episodic
990 Neoglacial Expansion and Rapid 20th Century Retreat of a Small Ice Cap on Baffin Island, Arctic Canada,
991 and Modeled Temperature Change." *Climate of the Past* 13 (11). [https://doi.org/10.5194/cp-13-1527-
992 2017](https://doi.org/10.5194/cp-13-1527-2017).
- 993 Pendleton, Simon L., Gifford H. Miller, Nathaniel Lifton, Scott J. Lehman, John Southon, Sarah E. Crump, and
994 Robert S. Anderson. 2019. Rapidly Receding Arctic Canada Glaciers Revealing Landscapes Continuously
995 Ice-Covered for More than 40,000 Years. *Nature Communications* 10 (1): 1–8.
996 <https://doi.org/10.1038/s41467-019-08307-w>.
- 997 Pendleton, Simon, Gifford Miller, Nathaniel Lifton, and Nicolás Young. 2019. Cryosphere Response Resolves
998 Conflicting Evidence for the Timing of Peak Holocene Warmth on Baffin Island, Arctic Canada." *Quaternary
999 Science Reviews* 216: 107–15. <https://doi.org/10.1016/j.quascirev.2019.05.015>.
- 1000 Ramsey, Christopher Bronk, Richard A. Staff, Charlotte L. Bryant, Fiona Brock, Hiroyuki Kitagawa, Johannes Van
1001 Der Plicht, Gordon Scholaut, et al. 2012. "A Complete Terrestrial Radiocarbon Record for 11.2 to 52.8 Kyr
1002 B.P." *Science* 338 (6105): 370–74. <https://doi.org/10.1126/science.1226660>.



- 1003 Rantanen M, Karpechko AY, Lipponen A, Nordling K, Hyvärinen O, Ruosteenoja K, Vihma T, Laaksonen A. 2022.
1004 The Arctic has warmed nearly four times faster than the globe since 1979. *Communications Earth &*
1005 *Environment* **3**: 168.
- 1006 Reimer, Paula J., William E.N. Austin, Edouard Bard, Alex Bayliss, Paul G. Blackwell, Christopher Bronk Ramsey,
1007 Martin Butzin, et al. 2020. "The IntCal20 Northern Hemisphere Radiocarbon Age Calibration Curve (0-55
1008 Cal KBP)." *Radiocarbon* 62 (4): 725–57. <https://doi.org/10.1017/RDC.2020.41>.
- 1009 Schweinsberg, A.D., J.P. Briner, G.H. Miller, O. Bennike, and E.K. Thomas. 2017. "Local Glaciation in West
1010 Greenland Linked to North Atlantic Ocean Circulation during the Holocene." *Geology* 45 (3).
1011 <https://doi.org/10.1130/G38114.1>.
- 1012 Schweinsberg, Avriël D, Jason P Briner, Gifford H Miller, Nathaniel A Lifton, Ole Bennike, and Brandon L Graham.
1013 2018. "Holocene Mountain Glacier History in the Sukkertoppen Iskappe Area , Southwest Greenland." *Quaternary Science Reviews* 197: 142–61. <https://doi.org/10.1016/j.quascirev.2018.06.014>.
- 1015 Serreze, M. C., A. P. Barrett, J. C. Stroeve, D. N. Kindig, and M. M. Holland. 2009. "The Emergence of Surface-
1016 Based Arctic Amplification." *Cryosphere* 3 (1): 11–19. <https://doi.org/10.5194/tc-3-11-2009>.
- 1017 Sigl, M. et al. 2015. Timing and climate forcing of volcanic eruptions for the past 2,500 years. *Nature* 523, 543–
1018 549.
- 1019 Søndergaard, Anne Sofie, Nicolaj Krog Larsen, Jesper Olsen, Astrid Strunk, and Sarah Woodroffe. 2019. "Glacial
1020 History of the Greenland Ice Sheet and a Local Ice Cap in Qaanaaq, Northwest Greenland." *Journal of*
1021 *Quaternary Science* 34 (7): 536–47. <https://doi.org/10.1002/jqs.3139>.
- 1022 Taylor, K. E., R. J. Stouffer, and G. A. Meehl, 2012: An Overview of CMIP5 and the Experiment Design. *Bull. Amer.*
1023 *Meteor. Soc.*, 93, 485–498, <https://doi.org/10.1175/BAMS-D-11-00094.1>. Tepes, P., Gourmelen, N.,
1024 Nienow, P., Tsamados, M., Shepherd, A. and Weissgerber, F., 2021. Changes in elevation and mass of Arctic
1025 glaciers and ice caps, 2010–2017. *Remote Sensing of Environment*, 261, p.112481.
1026 <https://doi.org/10.1016/j.rse.2021.112481>
- 1027 Werner, Johannes P., Dmitry V. Divine, Fredrik Charpentier Ljungqvist, Tine Nilsen, and Pierre Francus. 2018.
1028 "Spatio-Temporal Variability of Arctic Summer Temperatures over the Past 2 Millennia." *Climate of the*
1029 *Past* 14 (4): 527–57. <https://doi.org/10.5194/cp-14-527-2018>.
- 1030 Williams, L. D. 1978. "The Little Ice Age Glaciation Level on Baffin Island, Arctic Canada." *Palaeogeography,*
1031 *Palaeoclimatology, Palaeoecology* 25 (3): 199–207. [https://doi.org/10.1016/0031-0182\(78\)90036-6](https://doi.org/10.1016/0031-0182(78)90036-6).
- 1032 Wolken, Gabriel J., John H. England, and Arthur S. Dyke. 2005. "Re-Evaluating the Relevance of Vegetation
1033 Trimlines in the Canadian Arctic as an Indicator of Little Ice Age Paleoenvironments." *Arctic* 58 (4): 341–
1034 53. <https://doi.org/10.14430/arctic448>.
- 1035 Xu, Y., Lin, L., Diao, C., Wang, Z., Bates, S., & Arblaster, J. (2022). The response of precipitation extremes to the
1036 twentieth- and twenty-first-century global temperature change in a comprehensive suite of CESM1 large
1037 ensemble simulation: Revisiting the role of forcing agents vs. the role of forcing magnitudes. *Earth and*
1038 *Space Science*, 9, e2021EA002010. <https://doi.org/10.1029/2021EA002010>
- 1039 Zhao, Alcide, David S. Stevenson, and Massimo A. Bollasina. 2019. "Climate Forcing and Response to Greenhouse
1040 Gases, Aerosols, and Ozone in CESM1." *Journal of Geophysical Research: Atmospheres* 124 (24): 13876–
1041 94. <https://doi.org/10.1029/2019JD030769>.

<https://doi.org/10.5194/egusphere-2023-737>

Preprint. Discussion started: 2 May 2023

© Author(s) 2023. CC BY 4.0 License.



1042 Zhong, Y., A. Jahn, G. H. Miller, and A. Geirsdottir. 2018. "Asymmetric Cooling of the Atlantic and Pacific Arctic
1043 During the Past Two Millennia: A Dual Observation-Modeling Study." *Geophysical Research Letters* 45 (22):
1044 12,497-12,505. <https://doi.org/10.1029/2018GL079447>.